Equations for shear design and crack width control of deep beams

Auteur : Biada Kemadjou, Greg Freddy
Promoteur(s) : Mihaylov, Boyan
Faculté : Faculté des Sciences appliquées
Diplôme : Master en ingénieur civil des constructions, à finalité spécialisée en "civil engineering"
Année académique : 2024-2025
URI/URL : http://hdl.handle.net/2268.2/23359

Université de Liège
Faculté des Sciences Appliquées
Année académique 2024–2025

Equations for shear design and crack width control of deep beams

Master thesis submitted in fulfillment of the requirements for the Master Degree in Civil Engineering

Biada Kemadjou Greg Freddy

Promotor
Mihaylov Boyan

Jury members
Nenad Bijelic
Jean-François Demonceau
Frédéric Gens

Liège
June 2025

Acknowledgements

First and foremost, I would like to express my sincere gratitude to my promotor Boyan Mihaylov, for his constant help, insightful guidance, and availability throughout the preparation of this master thesis. His methodological rigor, critical thinking, and kindness were essential to the successful completion of this work.

I also extend my thanks to the members of the jury who will take the time to read and evaluate this thesis. Their expertise and critical perspective are a valuable asset to the recognition of this study, and I am grateful for the attention they will devote to it.

Finally, I would like to thank my family and friends for their unwavering support, patience, and encouragement throughout this journey. Their presence, both emotionally and morally, has been a vital foundation during moments of doubt as well as success.

Abstract

Deep beams in concrete infrastructures work mainly in shear. It is therefore important to assess the shear resistance of such a beam, as well as the evolution of the diagonal shear crack that develops on it, with a view to taking adequate measures to ensure its compliance during its service life. This work is therefore divided into an Ultimate Limit State study and a Serviceability Limit State study of deep beams; and more precisely of simply supported deep beams subjected to point loads. At Ultimate Limit States, the aim is to define relatively simple closed-form design equations against shear failure as in the case of slender beams. These equations are obtained by simplifying the full process established on the Two-Parameter Kinematic Theory which predicts the shear strength of a deep beam based on four components: the critical loading zone (CLZ), the aggregate interlock, the stirrups and the dowel action. The simplifications made to this method are designed to make it non-iterative, and to reduce the number of shear strength components from four to three by neglecting the dowel action contribution. At Serviceability Limit States, the aim is to establish a relationship between the applied shear and the width of the critical diagonal crack, in order to predict it at each loading stage of the beam. The approach developed is based on a rapid crack-based assessment model which enables to evaluate the residual shear capacity of a deep beam through three on-site measurements and two simple closed equations. It incorporates a crack-control effect likely to develop in some deep beams, so as to gain greater accuracy in predicted crack-width values.

Contents

List of Figures

List of Tables

Chapter 1

Introduction

1.1 Context and motivation

Deep beams are a special category of reinforced or prestressed concrete structural elements, mainly used in structures where high loads (generally concentrated loads) have to be carried over a short distance, while ensuring high rigidity and limited deformation.

They are widely used in various areas of construction, including bridge headers, interconnected foundation footings and transfer girders in large buildings.

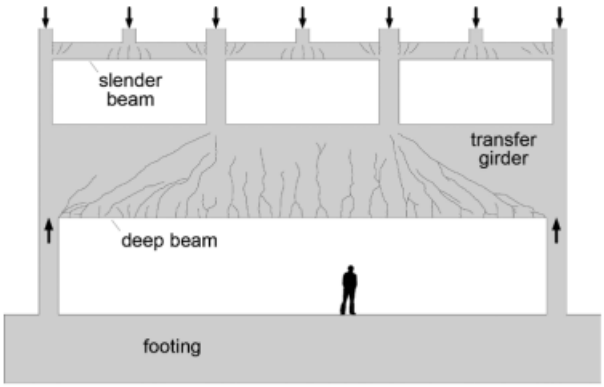

Figure 1.1: Slender and deep beam in a building [1].

These beams are characterised by a short span relative to their height. This geometric configuration results in a non-linear stress distribution and renders inapplicable the classical assumptions of Bernoulli's theory of bending, in particular that of the conservation of plane sections first demonstrated by Robert Hooke in 1678, and used to predict the load-deflection response of slender beams.

The first rigorous, structured study of deep beams is attributed to German researchers Leonhardt and Walther, who in the 1960s analysed the non-linear behavior of these elements and highlighted the inadequacy of conventional methods based on bending for this type of structure. They were among the first to propose a model based on the strut-and-tie method, which provides a better understanding of the actual path of internal forces between the load application zones and the supports. This concept was subsequently widely developed and

formalised by Jörg Schlaich, another German engineer, who in the 1980s introduced a systematic formulation of the strut-and-tie model for discontinuous zones in reinforced concrete, including deep beams. This model was subsequently incorporated into several design codes, including ACI 318 (USA) and Eurocode 2 (Europe).

Because of the relatively low span-to-height ratio of these beams (a/d ratio generally between 1.20 and 2.30), they work mainly in shear. Therefore, other theoretical models based on a prediction of the deformation patterns and using equilibrium, compatibility, and stress-strain relationships are used to predict the shear behavior of deep beams in an analogous way to the plane-sections theory for flexure, as the Two-Parameter Kinematic Theory (2PKT), which enables engineers to evaluate safety and assess deformations and crack widths of deep reinforced concrete beams such as the transfer girder in Figure 1.1.

Given that deep beams work mainly under large concentrated loads in concrete infrastructure, they often exhibit wide diagonal shear cracks that extend from the supports to concentrated loads during their services life. Therefore, in order to prevent these cracks from developing unacceptably during the service life of the beam, for example by carrying out early maintenance and strengthening techniques, it is necessary to be able to predict their evolution by correlating their width with the applied service loads.

1.2 Objectives of the thesis

The first purpose of this master thesis is to simplify the Two-Parameter Kinematic Theory (2PKT) in order to predict the shear strength of deep beams using closed-form design equations, such as those used for slender beams.

The second purpose is to use a model on rapid crack-based assessment (CBA) based on a single crack measurement which assesses the residual shear capacity of a deep beam, combined with the Two-Parameter Kinematic Theory with the aim of predicting the widening of shear cracks following applied loads over the service life of the deep beam.

1.3 Thesis outline

The following work is composed of five chapters, an appendix, and a bibliography.

Chapter 2 presents the backgrounds used for the work. The first part of this chapter explained the Two-Parameter Kinematic Theory for Shear Behavior of Deep Beams developed by Boyan I. Mihaylov, Evan C. Bentz, and Michael P. Collins as the simplified approach with closed-form design equations is based on it.

The second part presents a rapid crack-based assessment approach of deep beams based on a single crack measurement developed by Boyan Mihaylov, Eissa Fathalla ,and Alexandru Trandafir. Combined with the 2PKT, these two models are used to establish the approach proposed in this work for predicting crack widths in a deep beam.

Chapter 3 presents a simplified 2PKT approach for predicting the shear strength components of a deep beam. On the basis of justified assumptions, closed-form equations giving

the shear resistance of a deep beam are obtained in the same way as for a slender beam.

Chapter 4 presents a model based on the combination of the Two-Parameter Kinematic Theory and a rapid crack-based assessment of deep beams based on a single crack measurement for assessing the width of diagonal shear cracks in a deep beam in service.

Chapter 5 summarizes the conclusions that can be drawn from this study, and presents perspectives for improving the approaches developed.

Chapter 2

Backgrounds

This chapter draws primarily on the paper by Boyan I. Mihaylov, Evan C. Bentz, and Michael P. Collins published in 2013 on Two-Parameter Kinematic Theory for Shear Behavior of Deep Beams [1], as well as the paper by Boyan Mihaylov, Eissa Fathalla, and Alexandru Trandafir published in 2024 on Rapid crack-based assessment of deep beams based on a single crack measurement [2].

2.1 Two-Parameter Kinematic Theory for Shear Behaviour of Deep Beams

The Two-Parameter Kinematic Theory for shear behavior of Deep Beams is a kinematic model capable of predicting the deformed shape of deep beams on the basis of two degrees of freedom (DOFs). Indeed, the fundamental hypothesis for slender beams that "plane sections remain plane" is not applicable for this type of beam, since plane sections no longer remain plane, as shown in figure 2.1(d). Shear deformations become dominant and the deformation mode much more complex.

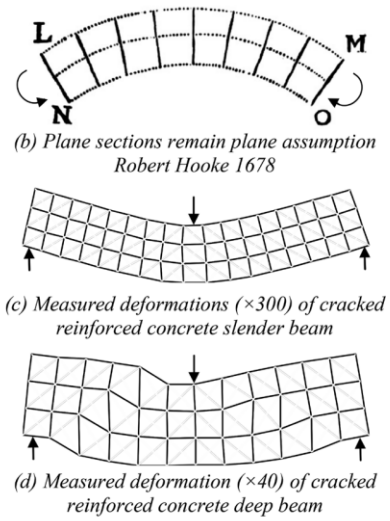

Figure 2.1: Deformation patterns of slender beams and deep beams [1].

Combined with equilibrium equations and stress-strain relationships, the 2PKT model can be used to predict the shear strength and deformation patterns of deep beams at shear

failure. This deformation mode includes crack widths, maximum deflections, and the complete displacement field for the beam.

2.1.1 Kinematics of Deep Beams

The model is based on only two degrees of freedom capable of describing the deformed shape of diagonally-cracked point-loaded deep beams subjected to single curvature.

The model assumes that the critical crack extends from the inner edge of the support to the far edge of the tributary area of the loading plate responsible for the shear force V. The concrete above this crack is modeled as a rigid block, while the concrete below the crack is modeled as a series of rigid radial struts ($\epsilon_r = 0$), connecting the loading point to the bottom longitudinal reinforcement. These two regions on either side of the critical crack are connected by the critical loading zone (CLZ) at the top of the section, by the bottom flexural reinforcement and by the stirrups.

The basic assumption of this model is that the motion of the concrete block above the crack can be described by a rotation about the top of the crack and by a vertical translation (Figure 2.2(a)). This translation is equal to the vertical displacement Δ_c of the CLZ, while the rotation is proportional to the average strain in the bottom reinforcement $\epsilon_{t,avg}$. Thus, Δ_c and $\epsilon_{t,avg}$ represent the two degrees of freedom of this model (Figure 2.2(b)). The elongation of the bottom reinforcement causes the rotation of the rigid radial struts about the loading point and crack widening. Transverse displacement in the the critical loading zone causes both widening and slip displacement of the critical diagonal crack. As shown in Figure 2.2(b), the two degrees of freedom cause tensile strains in the transverse reinforcement.

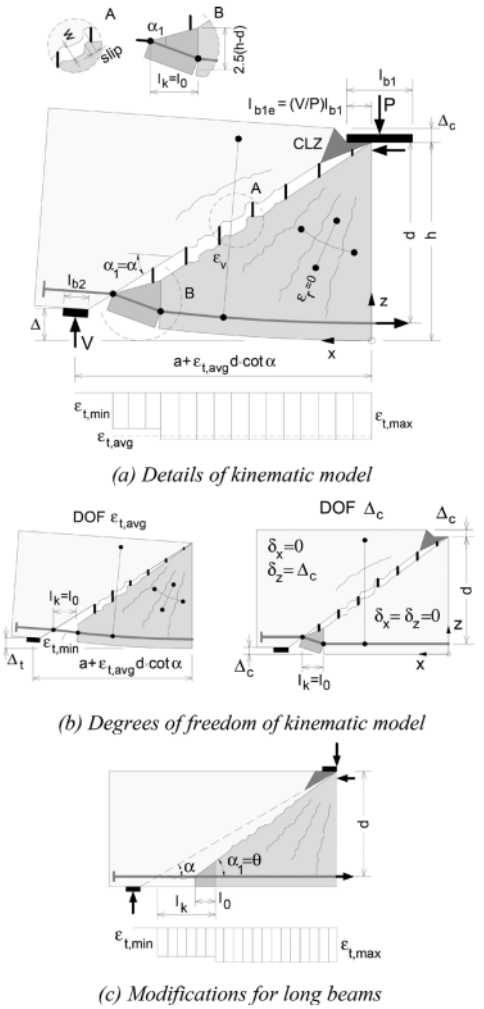

Figure 2.2: Kinematic model for deep beams [1].

Based on the aforementioned assumptions, the horizontal and vertical displacements of all points in the beam can be expressed from the two degrees of freedom as follows :

- Points below the critical crack

$$\delta_x(x,z) = \epsilon_{t,avg} x \tag{2.1}$$

$$\delta_z(x,z) = \frac{\epsilon_{t,avg} x^2}{h-z} \tag{2.2}$$

- Points above the critical crack

$$\delta_x(x,z) = \epsilon_{t,avg}(h-d)\cot\alpha \tag{2.3}$$

$$\delta_z(x,z) = \epsilon_{t,avg} x \cot\alpha + \Delta_c \tag{2.4}$$

These displacements are with respect to the x-z axis system shown in figure 2.2(a). Thus, these equations describe the complete deformed shape of the beam, and can therefore be used to calculate the strain between any two points on the surface of the beam.

- **Critical diagonal crack.**

  This model can also be used to estimate the width of critical diagonal cracks. Based on figure 2.2, we show that:

$$w = \Delta_c \cos\alpha_1 + \frac{\epsilon_{t,min} l_k}{2 \sin\alpha_1} \tag{2.5}$$

  Where the two terms in this expression represent the contributions of the two DOFs. Quantity l_k in Eq.(2.5) is the length of the bottom reinforcement whose elongation contributes to the width of the critical crack, which is equals to the distance between the kinks that develop in the longitudinal bars near the support (Figure 2.2) and thus

$$l_k = l_0 + d(\cot\alpha - \cot\alpha_1) \tag{2.6}$$

$$l_0 = 1.5(h-d)\cot\alpha_1 \geq s_{max} \tag{2.7}$$

$$s_{max} = \frac{0.28 d_b}{\rho_l} \frac{2.5(h-d)}{d} \tag{2.8}$$

  where l_0 is the length of the heavily cracked zone at the bottom of the critical crack; s_{max} is the spacing of the radial cracks at the bottom of the section; and the quantity $2.5(h-d)$ is the approximate depth of interaction between the bottom bars and the surrounding concrete.

  Figure 2.3 shows that equation 2.5 takes fairly well into account all the parameters that influence crack width. The vertical axis shows the crack widths measured during the experimental study, while the vertical axis shows those calculated using equation 2.5.

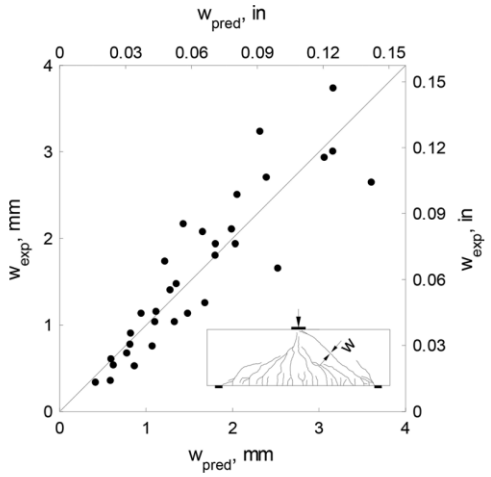

Figure 2.3: Predictions of kinematic model for crack widths [1].

2.1.2 Critical Loading Zone

The critical loading zone (CLZ) represents a key component of the two-parameter kinematic theory.

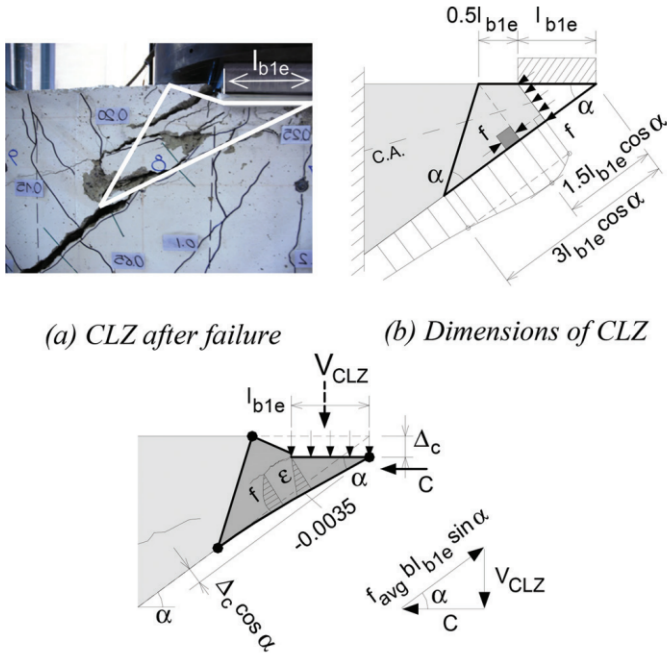

Figure 2.4: Modeling of CLZ [1].

Figure 2.4(a) shows a photograph of the critical loading zone of one of the specimens of the experimental study after failure. The spalled concrete and the orientation of the cracks in this zone indicate that it failed due to high diagonal compressive stresses.

The CLZ can be idealized by a variable-depth elastic cantilever fixed at one end and loaded at the other shown in figure 2.4(b). Analysis of this model shows that the compressive stress along the bottom edge of the cantilever reaches its maximum value at a distance of $1.5l_{b1e}\cos\alpha$ from the tip section and returns to the applied stress at a distance of $3l_{b1e}\cos\alpha$ from the same section. This result makes it possible to define a triangular critical loading zone with a bottom length of $3l_{b1e}\cos\alpha$ and a top vertex located opposite to the location of the maximum compressive stress.

Knowing the geometry of the critical loading zone, the ultimate shear displacement Δ_c can be calculated by assuming values for the average strains along the bottom and top sides of this zone (refer to Figure 2.4(c)). As the zone fails due to combined moment and compression, the bottom strain is assumed equal to –0.0035 and the top strain is assumed equal to zero. Using these values, it can be shown that

$$\Delta_c = 0.0105 l_{b1e} \cot\alpha \tag{2.9}$$

The appropriateness of Eq. (2.9) is illustrated in Figure 2.5, which shows the relationship between the shear force and the measured shear displacement of the critical loading zones

of eight specimens of the experimental study. It can be seen that the experimental results agree reasonably well with the predictions.

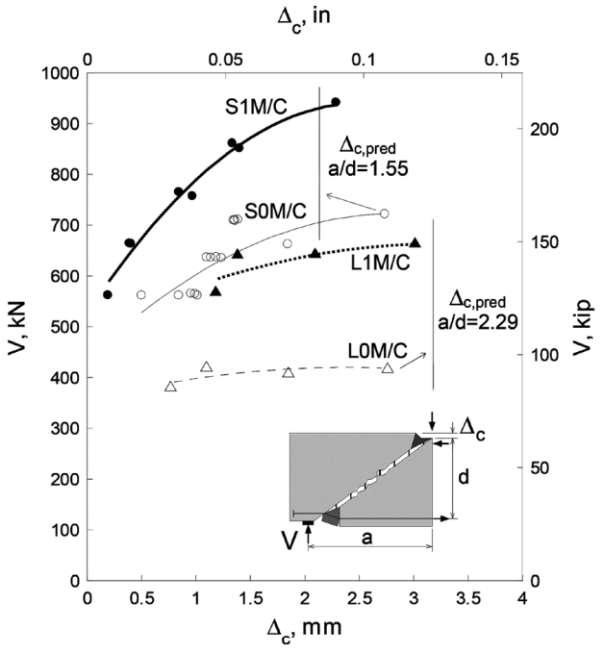

Figure 2.5: CLZ: test results and predictions [1].

The shear capacity of the critical loading, V_{CLZ}, can be derived with the help of Figure 2.4(c), where it is assumed that the compressive strain ϵ varies linearly from zero at the edge of the loading plate to –0.0035 just above the critical crack. The average compressive stress from this strain profile is thus

$$f_{avg} = \frac{\Omega_0}{0.0035} \approx 1.43 f_c'^{0.8} [Mpa] \tag{2.10}$$

where Ω_0 is the area under the stress-strain curve of concrete in uniaxial compression taken up to a strain of –0.0035. Considering the triangle of forces shown in Figure. 2.4(c), the shear strength of the critical loading zone is expressed as

$$V_{CLZ} = k f_{avg} b l_{b1e} \sin^2 \alpha \tag{2.11}$$

where k is a crack shape coefficient which accounts for the fact that, in slender beams, the critical diagonal crack is not straight but has an S-shape and approaches the loading plate at a very flat angle.. Based on comparisons with tests, it is suggested that $k = 1$ for beams with $\cot \alpha \leq 2$ and $k = 0$ for beams with $\cot \alpha \geq 2.5$, with a linear transition for intermediate values of $\cot \alpha$.

Figure 2.5 also shows very high values of shear resistance at a very small value of Δ_c. This shows that a significant part of the shear in deep beams is carried by mechanisms other than diagonal compression in the critical loading zones.

2.1.3 Other shear strength components in deep beams

2.1.3.1 Shear Resisted by Aggregate Interlock

Due to the displacement Δ_c, the critical diagonal crack undergoes widening and a significant slip displacement, as Detail A in Figure 2.2(a) shows. Due to aggregate interlock, this slip will generate significant shear stresses contributing to the shear resistance of the member.

The shear resisted by aggregate interlock is expressed as

$$V_{ci} = \frac{0.18\sqrt{f'_c}}{0.31 + \frac{24w}{a_{ge}+16}} \cdot bd \tag{2.12}$$

where the effective aggregate size a_{ge} equals a_g for concrete strengths less than 60 MPa and zero for strengths larger than 70 MPa with a linear transition for intermediate strengths, and the crack width w is calculated from Eq. (2.5) using the following simplification :

$$\epsilon_{t,min} \approx \epsilon_{t,max} = \frac{T_{max}}{E_s A_s} = \frac{Va}{E_s A_s (0.9d)} \tag{2.13}$$

where T_{max} is the tension force in the flexural reinforcement at the section with maximum bending moment.

2.1.3.2 Shear Resisted by Stirrups

The shear resisted by the stirrups is calculated from

$$V_s = \rho_s b(d \cot \alpha_1 - l_0 - 1.5 l_{b1e}) f_v \tag{2.14}$$

where the expression in the brackets represents the length along the shear span within which the critical crack is wide enough to cause significant tension in the stirrups (refer to Figure 2.6). The stress in the stirrups is calculated by assuming elastic-perfectly plastic behavior of the steel :

$$f_v = E_s \epsilon_v \leq f_{yv} \tag{2.15}$$

where the transverse strain at the middle of the shear span, ϵ_v, is derived from the kinematic model :

$$\epsilon_v = \frac{1}{0.9d}(\Delta_c + 0.25\epsilon_{t,avg} d \cot^2 \alpha_1) \approx \frac{1.5\Delta_c}{0.9d} \tag{2.16}$$

2.1.3.3 Shear Resisted by The Dowel Action

As we can see in Detail B in Figure 2.2(a), the bottom longitudinal bars in deep beams are subjected to double curvature near the support and thus will resist shear by dowel action. The dowels of length l_k can be very effective, as at one end they push upon the support plate and at the other end upon the concrete of the web.
So, the shear resisted by the dowel action of the bottom reinforcement is calculated from

$$V_d = n_b f_{ye} \frac{d_b^3}{3l_k} \tag{2.17}$$

where n_b is the number of bars, and d_b is the bar diameter. This expression is derived by assuming that the dowels of length l_k (Eq. (2.6)) work in double curvature with plastic hinges forming at each end. The moment capacity of the hinges is calculated with an effective yield strength f_{ye} to account for the effect of the tension in the bars.

$$f_{ye} = f_y[1 - (\frac{T_{min}}{f_y A_s})^2] \leq 500[Mpa] \tag{2.18}$$

where the tension force in the reinforcement near the support, T_{min}, can be replaced by T_{max} from Eq. (2.13) for simplicity, and the limit of 500 MPa in Eq. (2.18) accounts approximately for the fact that the transverse displacement at the dowel may not be sufficiently large to cause plastic hinges in bars with high yield strength.

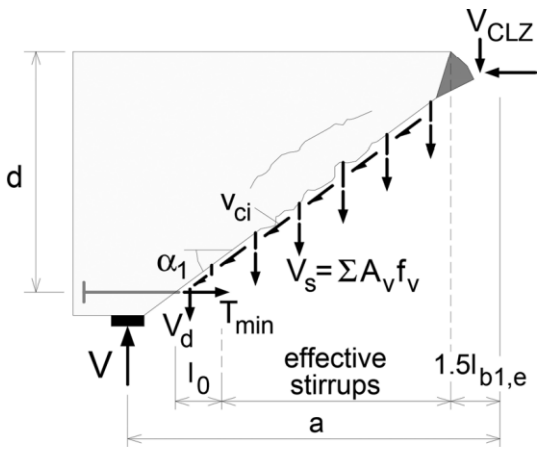

Figure 2.6: Shear strength components in deep beam [1].

2.1.4 Shear Strength of Deep Beams

The shear resistance of deep beams can be expressed as

$$V = V_{CLZ} + V_{ci} + V_s + V_d \tag{2.19}$$

as the free body diagram in Figure 2.6 shows. V_{CLZ}, V_{ci}, V_s, and V_d are the shear forces resisted by the critical loading zone, by aggregate interlock, by stirrups, and by dowel action respectively.

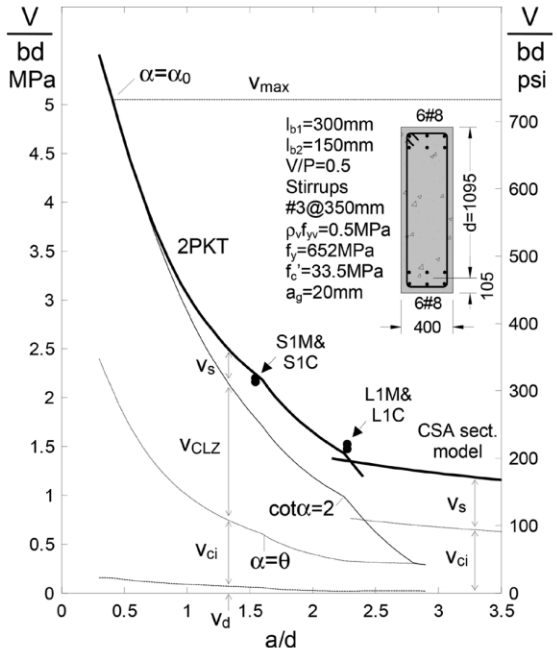

Figure 2.7: Predicted shear strength components for different a/d [1].

Figure 2.7 summarizes the predicted components of shear strength and how these components change with the a/d for beams having the same section as that used in the experimental program.

For deep beams, the concrete contribution $V_{CLZ} + V_{ci}$ varies from 67% when $a/d = 2.3$ up to 97% at $a/d = 0.5$, with the dowel force provided by the longitudinal reinforcement accounting for the remaining 3% of the shear strength.

As a/d increases, the angle of the critical crack will decrease, resulting in a larger stirrup contribution V_s as more stirrup legs cross the critical crack. At the same time, the shape of the critical loading zone becomes more slender, reducing both its strength V_{CLZ} and its stiffness. The reduction in stiffness results in a wider critical crack, and thus lower aggregate interlock contribution V_{ci} as a/d increases.

2.1.4.1 The Size Effect

The 2PKT method gives a better understanding of the size effect in deep beams, which was an important motivation for the development of the model. In fact, The components of shear resistance V_{CLZ}, V_{ci}, and V_d for the beams without stirrups predict that the size effect in deep beams is caused mainly by aggregate interlock. As the member size increases, the larger critical loading zone deforms more, causing wider diagonal cracks that in turn result in diminishing shear stresses transferred across the cracks.

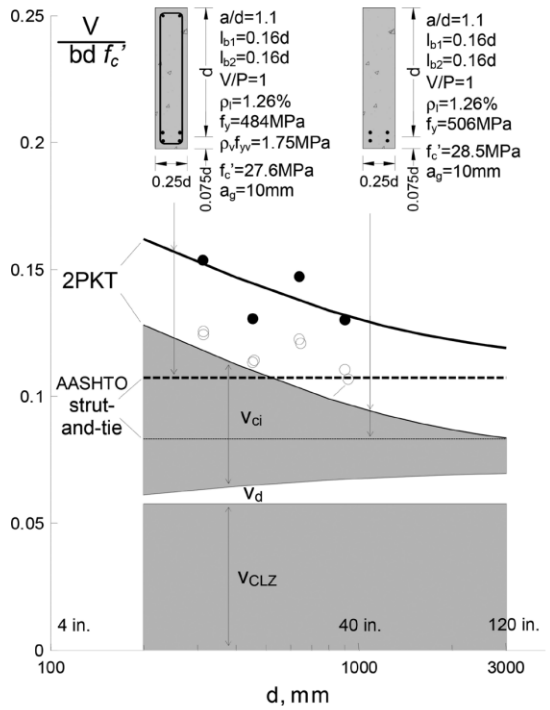

Figure 2.8: Size effect in deep beams: theoretical predictions and experimental results [1].

Figure 2.8 compares the shear strength predictions to the results of 12 size effect tests by Zhang and Tan. Eight of the specimens were without web reinforcement (hollow dots) and four of the specimens contained 0.41% of stirrups (solid dots). As we can see in that figure, the 2PKT captures well the size effect contrary to AASHTO strut-and-tie model, which does not account for the size effect and provides an approximate lower bound to the predictions of the 2PKT method. For these beams, the ACI strut-and-tie model, which also neglects the size effect, produces similar predictions.

2.1.5 Comparison of the 2PKT Method with Other Methods

Other predictions similar to those made in the experimental study were made on a total of 434 tests published on simply supported beams with a/d between 0.5 and 3, and the results are summarized in Figure 2.9.

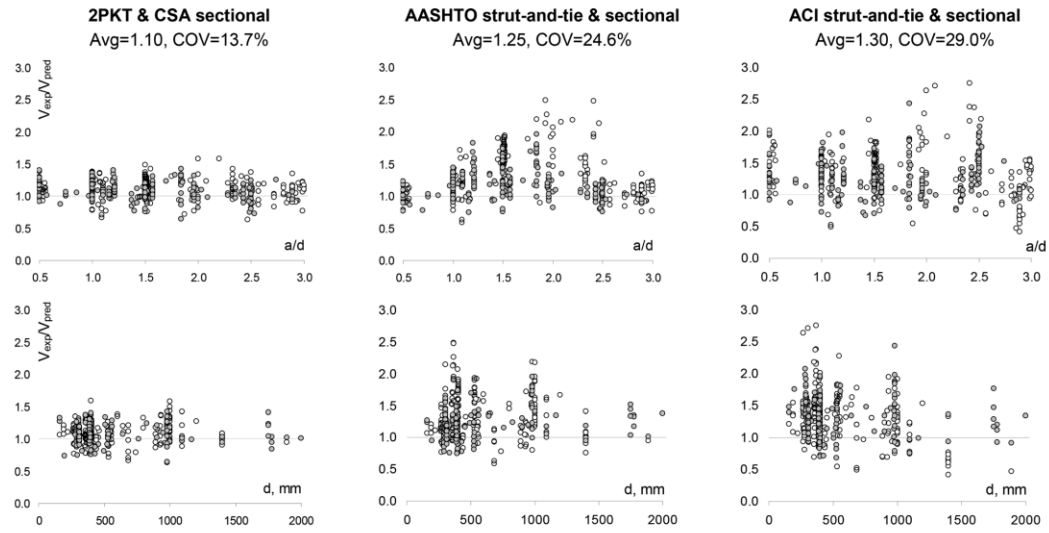

Figure 2.9: Comparison between 2PKT, AASHTO, and ACI shear previsions for 434 tests [1].

Also shown in this figure are the ratios of experimental to predicted shear strengths given by the AASHTO and ACI codes. The top three plots show the ratios of experimental to predicted shear strengths as a function of a/d, while the bottom three plots show the same ratios as a function of the effective depth d. It can be seen that the 2PKT method provides significantly more consistent predictions than the two design codes across the entire range of a/d and d values. The predictions of the AASHTO code have a large number of conservative values for a/d between 1 and 2.5 and it is in this region that the 2PKT method provides the most significant improvement in accuracy. Because the ACI code does not account for the size effect in shear, there is a clear decrease in conservatism as member depth increases.

2.1.6 Conclusion on the Two-Parameter Kinematic Theory (2PKT)

The two-parameter kinematic theory (2PKT) presented in this paper is capable of predicting the shear failure load, the crack widths near failure, and the complete deformed shapes of diagonally cracked point-loaded deep beams subjected to single curvature. A key component of the 2PKT is the modeling of the critical loading zone which is the area of highly stressed concrete near the point of load application. The ultimate vertical displacement of this zone is one of the two kinematic parameters of the model, while the other is the average tensile strain in the longitudinal reinforcement on the flexural tension side. The theory allows for the components of shear resistance of deep beams to be evaluated at failure.

2.2 Rapid Crack-Based Assessment of Deep Beams based on a Single Crack Measurement

At failure, deep beams often exhibit wide diagonal shear cracks extending from the supports to the concentrated loads. During the service life of the beam, this diagonal crack widens, reducing the stiffness of the beam and therefore its residual capacity, which corresponds to the additional load that the beam can still support before it completely fails. Knowing the residual strength of the beam during its service life would therefore enable it to be maintained over the long term. For deep beams in bridges for example, this would make

it possible to reinforce the structure or remove lanes depending on traffic loads, and thus prevent the bridge from collapsing.

2.2.1 Introduction

The model presented here can be used to assess the residual capacity of a deep beam in service on the basis of its condition.

Based on three input parameters, this model can be used to assess the residual capacity of a deep beam in service. It is based on the Two-Parameter Kinematic Theory (2PKT) presented above, the key element of which is the the critical loading zone (CLZ). The three input parameters correspond to three on-site measurements: the depth of the critical loading zone (CLZ) determined by the diagonal crack; the angle of the crack in the CLZ; and the vertical crack displacement in the vicinity of the CLZ. Knowing these data, the model establishes a relationship between the crack opening and the residual strength expressed as a percentage of the ultimate shear strength of the deep beam through two relatively simple closed-form equations.

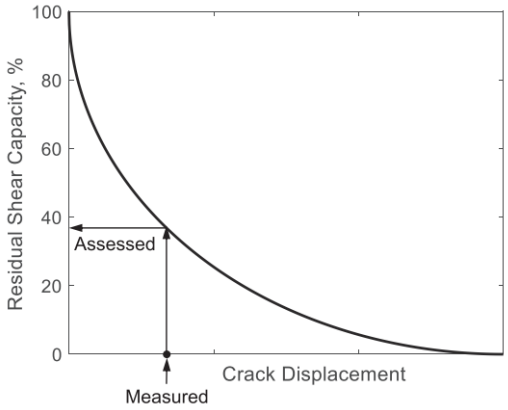

Figure 2.10: Residual shear capacity diagram for direct crack-based assessment [2].

The more the beam is loaded, the wider the crack and the lower the stiffness of the beam, and therefore the additional load that the beam can support before its failure decreases. So, from this simple physical understanding, it can be seen that the residual strength decreases with the opening of the crack and is zero when the beam supports its maximum load (shear failure). This is shown in figure 2.10.

The aim of this model is therefore to draw up diagrams such as the one in Figure 2.10 in advance, which, based on the measurement of the crack displacement, allow the residual capacity of the beam to be rapidly assessed and appropriate measures to be taken.

2.2.2 Experimental observations and 2PKT Analysis

In order to answer important questions about the crack-based assessment and to develop the model presented here, an experimental study was carried out on a specimen named P8.

2.2.2.1 Experimental observations

Three loading-unloading cycles were performed on the beam, increasing the load at each loading but maintaining the unloading at the same level.

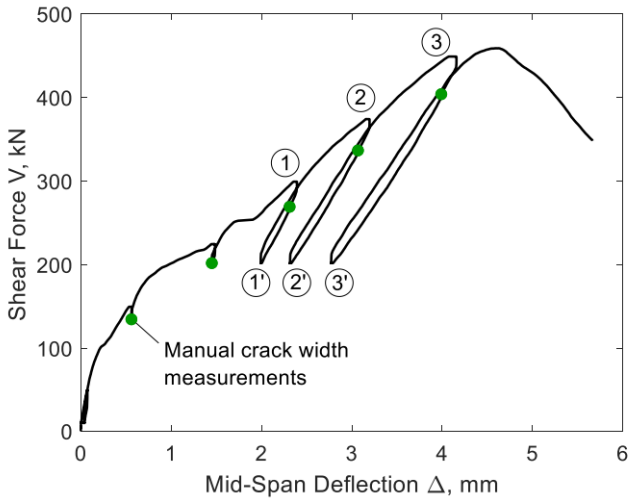

Figure 2.11: Global response of the specimen [2].

Points 1, 2 and 3 correspond respectively to peak loads of 300kN, 375kN and 450kN during each loading cycle, while points 1', 2' and 3' correspond to unloading at 200kN.

Major diagonal cracks formed at a shear force corresponding to approximately 49% of the shear strength. The failure then occurred at a load $V = V_u = 459kN$ by a sudden widening of the diagonal crack on the east side and by the crushing of the concrete above the critical crack near the edge of the loading plate.

This zone of high damage corresponds to the critical loading zone (CLZ) as it typically triggers the failure of deep beams, as seen in the 2PKT model above. Following this observation, the CLZ emerges as the key element for developing a rapid crack-based assessment (CBA) approach.

The deformations of the critical loading zone were therefore captured during the three loading-unloading cycles and studied.

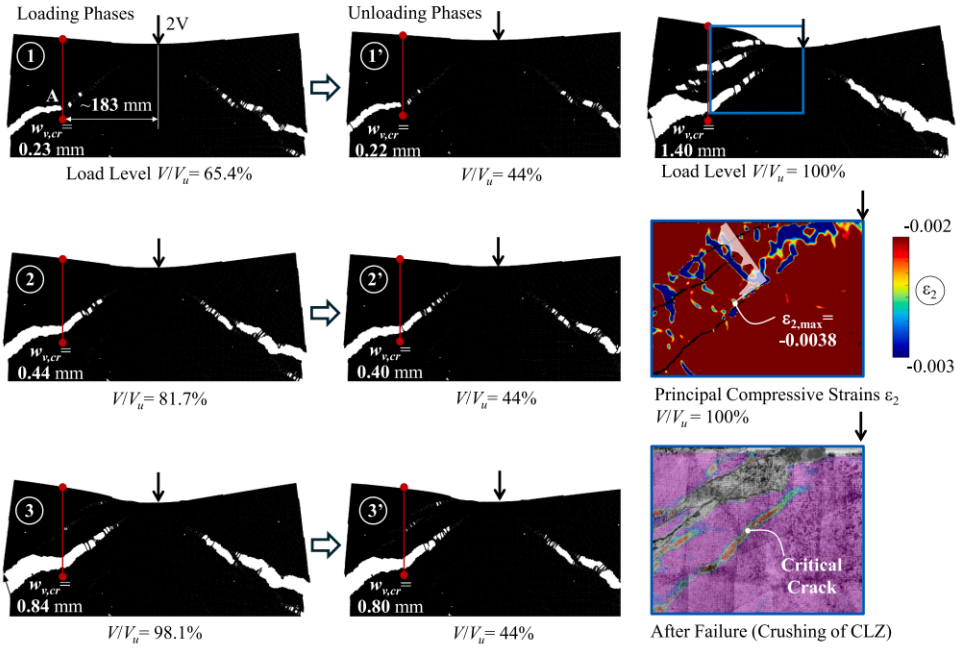

Figure 2.12: Deformations in the critical loading zone [2].

The diagrams in figure 2.12 show clear shear distortions of the critical loading zone, particularly at 98.1% of V_u when inclined macrocracks formed in the CLZ due to high diagonal compressive stresses. Shear deformations mainly result in vertical displacements of critical diagonal cracks in the vicinity of the load, denoted $w_{v,cr}$.

It can be seen also that as we go from one charge cycle to the next, i.e. as we increase the load, $w_{v,cr}$ increases quite visibly, whereas at each discharge, $w_{v,cr}$ is recovered weakly. This is an important property of the critical vertical crack displacement.

2.2.2.2 2PKT analysis

The behavior of this experimental specimen is then modelled and studied using the crack-based assessment approach which is based on the 2PKT model presented above. In this way, the CBA is applicable to shear-critical deep beams, which have developed complete diagonal cracks between the loading and support points, just like the 2PKT.

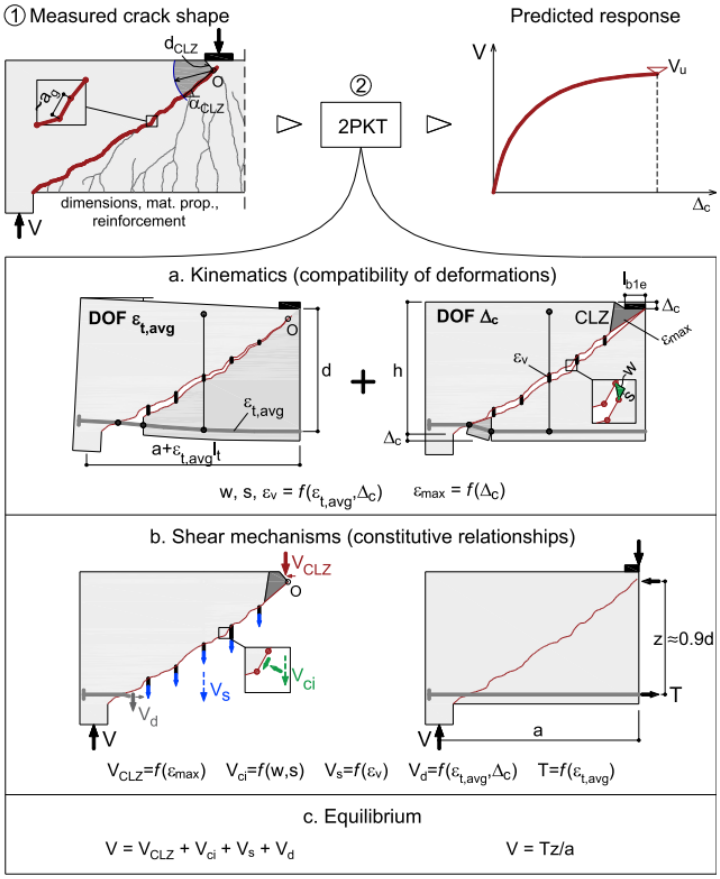

Figure 2.13: Summary of the CBA approach using the 2PKT [2].

Figure 2.13 shows the main stages of the CBA. Firstly, the geometry of the critical diagonal crack is measured on site. Secondly, this crack geometry and the main beam properties are used as input parameters to the 2PKT model in order to simulate the complete shear response of the beam up to failure.

Figure 2.13a-c summarises the 2PKT model seen in section 2.1.Thus, by solving the two equations in Figure 2.13c for a given shear force V, the two degrees of freedom $\epsilon_{t,avg}$ and Δ_c of the 2PKT model are obtained, and the Δ_c degree of freedom is used to predict the shear response of the beam.

The critical loading zone is a key element of the CBA approach. It is modelled as described in the 2PKT in section 2.1.2. Based on the modelling of the CLZ, its shear strength is expressed in the CBA approach as :

$$V_{CLZ} = \sigma_{avg} b d_{CLZ} \sin \alpha_{CLZ} \tag{2.20}$$

with σ_{avg} the average compressive stress in the CLZ which is equals to f_{avg} in the 2PKT model, $d_{CLZ} = l_{b1e} \sin \alpha_{CLZ}$, with α_{CLZ} the angle of the critical diagonal crack which corresponds to α_1 in the 2PKT. l_{b1e} is the effective width of loading plate parallel to longitudinal axis of member, as seen above in the 2PKT. By rearranging this expression of V_{CLZ}, we find the same expression as in the 2PKT model in equation 2.11 for $k = 1$ and by approximating α_1 by α. Indeed, k is a crack shape coefficient which allows the boundary between deep and slender beams to be taken into account in the 2PKT model. However, the CBA approach

applies exclusively to deep beams, for which $a/d \leq 2.3$ is generally the case and for which $k = 1$ is therefore required.

Equation 2.20 therefore shows that the prediction of the CLZ behavior is quite influenced by the values of d_{CLZ} and α_{CLZ}, which are very sensitive to random variations in the geometry of the critical diagonal crack. For this reason, d_{CLZ} and α_{CLZ} are obtained from the measured crack geometry in the CBA approach in order to maintain good accuracy.

In the 2PKT method, the Δ_c degree of freedom characterizes the deformation of the CLZ, whereas in the CBA approach, this deformation mainly results in the vertical displacement of the critical crack $w_{v,cr}$. It is therefore crucial to make a link between the two. By comparing figure 2.12 and the idealized deformation pattern in figure 2.13, it can be seen that the shear degree of freedom Δ_c is nearly identical to the vertical crack displacement $w_{v,cr}$, due to the fact that the strains along the bottom reinforcement ($\epsilon_{t,avg}$) has a negligible effect on the vertical crack displacement. To be more precise, $w_{v,cr}$ should be measured at the edge of the CLZ (at point A according to figure 2.12), as this is where the effect of $\epsilon_{t,avg}$ on $w_{v,cr}$ is most negligible.

Thus, the CBA approach presented in figure 2.13 can be used to predict the measured crack displacement at the edge of the CLZ as equals to Δ_c.

This CBA approach is implemented on the specimen of this experimental study.

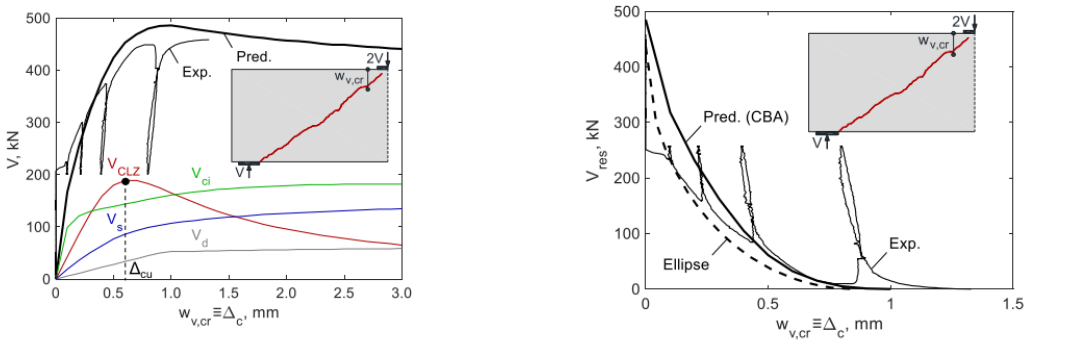

a) Measured and predicted critical crack displacement $w_{v,cr}$ b) Residual shear strength with an elliptical approximation

Figure 2.14: 2PKT analysis of the specimen [2].

The plot in figure 2.14a compares the predicted and measured response in terms of shear force V versus the critical vertical crack displacement $w_{v,cr} \equiv \Delta_c$. It can be seen that after each unloading, the vertical displacement of the crack is not recovered, as shown in figure 2.14. This is an important property of the model presented here. It can be seen also that the failure of the beam and the failure of the CLZ are almost coincident in terms of $w_{v,cr}$ values, which justifies that the shear failure of the deep beam is mainly defined by the failure of the CLZ, as stipulated above. Thus, based on these observations, it emerges that in order to predict $w_{v,cr}$ at the failure of the beam, it is only necessary to predict the displacement capacity of the CLZ, independently of the other shear mechanisms. This too is an important property for the development of the simplified CBA model.

Figure 2.14b presents the same information but in a different format. Mainly, it shows that at $\Delta_c = 0$, the residual shear strength $V_{res} = V_u$ the ultimate shear strength, and that

at $\Delta_c = \Delta_{cu}$ the vertical displacement capacity of the crack, the residual shear strength is zero ($V_{res} = 0$). These properties, and the elliptical shape of the curve, reflect the physics of the problem, as shown by the comparison between figures 2.10 and 2.14b.

Finally, and most importantly, a good agreement is achieved between the measured and predicted monotonic response in terms of envelope curves, reflecting a fairly good accuracy of the CBA approach compared to the experimental study.

This elliptical shape and an adequate prediction of Δ_{cu} are used to develop a simplified CBA approach.

2.2.3 Proposed novel simplified CBA for rapid assessment

2.2.3.1 Formulation of the simplified CBA

Based on observations made from the experimental study and the CBA-2PKT analysis of the specimen P8, a rapid and simplified approach of the CBA can be developed. It consists on a 5-step procedure:

1. Inspect the CLZ of the beam for inclined macrocracks. If this is the case, then the element is in distress and urgent measures must be taken to prevent its collapse.

2. If inclined cracks are not present, measure the geometry of the critical loading zone, more precisely the distance d_{CLZ} and the angle α_{CLZ}.

3. Calculate the displacement capacity of the CLZ Δ_{cu} as :

$$\Delta_{cu} = 0.009 d_{CLZ} \frac{\cos \alpha_{CLZ}}{\sin^2 \alpha_{CLZ}} \tag{2.21}$$

   This expression of Δ_{cu} is virtually the same as that proposed by the 2PKT model in equation 2.9, knowing that $d_{CLZ} = l_{b1e} \sin \alpha_{CLZ}$, approximating α_{CLZ} by α and replacing the constant 0.009 by 0.0105. Indeed, the CBA approach considers a compressive strain along the bottom face of the CLZ ϵ_{max} of $-3 * 10^{-3}$ versus $-3.5 * 10^{-3}$ in the 2PKT model.

4. Measure the critical vertical crack displacement $w_{v,cr}$ at the edge of the CLZ, i.e. at point A in figure 2.12.

5. Calculate the residual shear capacity of the beam ψ for the measured critical crack displacement $w_{v,cr}$. This residual capacity is expressed by :

$$\psi(w_{v,cr}) = (1 - \frac{V}{V_u}) * 100\% = 0.9[1 - \sqrt{1 - (1 - \frac{w_{v,cr}}{\Delta_{cu}})^2}] * 100\% \tag{2.22}$$

The first step in this procedure is justified by the fact that macrocracks develop close to failure, when the crushing of the critical loading zone is observed. The equation 2.22 is derived on the basis of the elliptical shape of the curve $V_{res} - w_{v,cr}$ and its properties, as seen in figure 2.14b above. The factor 0.9 is applied to this ellipse in equation 2.22 in order to introduce a certain conservatism into the estimation of the residual shear capacity.

As mentioned above, the critical crack displacement is not recovered after each unloading. Thus, $\psi(w_{v,cr})$ does not necessarily represent the residual shear capacity of the beam under the current loading, but rather that under the greatest load the beam has had to bear during its entire service life. Thus, this simplified CBA approach allows to take into account the beam's "memory" by keeping the maximum load it has experienced during its entire loading history.

2.2.3.2 Validation of the simplified CBA

The simplified and rapid crack-based assessment approach presented above is validated with various tests.

Beam	a/d[−]	d [mm]	ρ_l [%]	ρ_v [%]	f_c [MPa]	d_{CLZ} [mm]	α_{CLZ} [deg]	$\Delta_{\mathrm{cu,pred}}$ [mm]	$\Delta_{\mathrm{cu,exp}}$ [mm]	$V_{u,exp}$ [kN]
P8	1.64	732	1.37	0.134	39.7	54	41	0.85	1.40	459
P3	1.64	732	1.37	0.134	40.5	74	34	1.77	1.60	466
CCR2	2.00	1105	2.10	0.141	35.8	127	30	3.83	3.38	1118
PLS4000W	1.82	3840	0.66	0.080	44.2	123	32	3.29	3.47	1509
S1M	1.55	1095	0.70	0.101	33.0	59	36	1.25	-	941
S0M	1.55	1095	0.70	0	34.2	34	30	1.01	-	721

Table 2.1: Summary of beam properties [2].

with : a = shear span; d = effective depth; ρ_l = flexural reinforcement ratio; ρ_v = transverse reinforcement ratio; f_c = concrete compressive strength; d_{CLZ} = measured depth of critical loading zone; α_{CLZ} = measured angle of critical crack in critical loading zone; $\Delta_{cu,pred}$ = predicted displacement capacity of the CLZ using equation 2.21; $\Delta_{cu,exp}$ = measured displacement capacity of the CLZ ($w_{v,cr}$ at beam failure); $V_{u,exp}$ = measured shear strength.

The table in Figure 2.1 shows the main properties of the beams used for these tests.

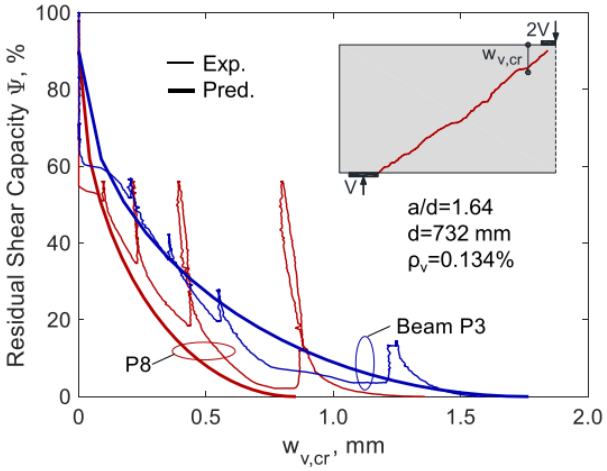

Figure 2.15: Measured and predicted residual capacity diagrams of nominally identical specimens P8 (red) and P3 (blue) [2].

Figure 2.15 compares the predicted and experimental residual shear capacities of specimens P8 and P3. These specimens are almost identical, differing only slightly in f_c (39.7MPa for P8 vs 40.5 Mpa for P3). However, the measured ψ curves are quite different. This is mainly due to α_{CLZ} and d_{CLZ} which are different because of random variations in the path of the critical cracks near the CLZ, as assumed above. Figure 2.15 therefore highlights the fairly significant influence of these two measured parameters on the Simplified CBA approach.

Also important, figure 2.15 demonstrates the fairly good accuracy of this simplified CBA model in predicting the residual shear capacity of the two specimens using few input parameters, with a good matching between predicted and experimental ψ curves.

Figure 2.16 below shows the predicted and experimental residual shear capacity curves for the four remaining specimens, which have quite different properties. It therefore provides further confirmation of the accuracy of this simplified crack-based assessment approach.

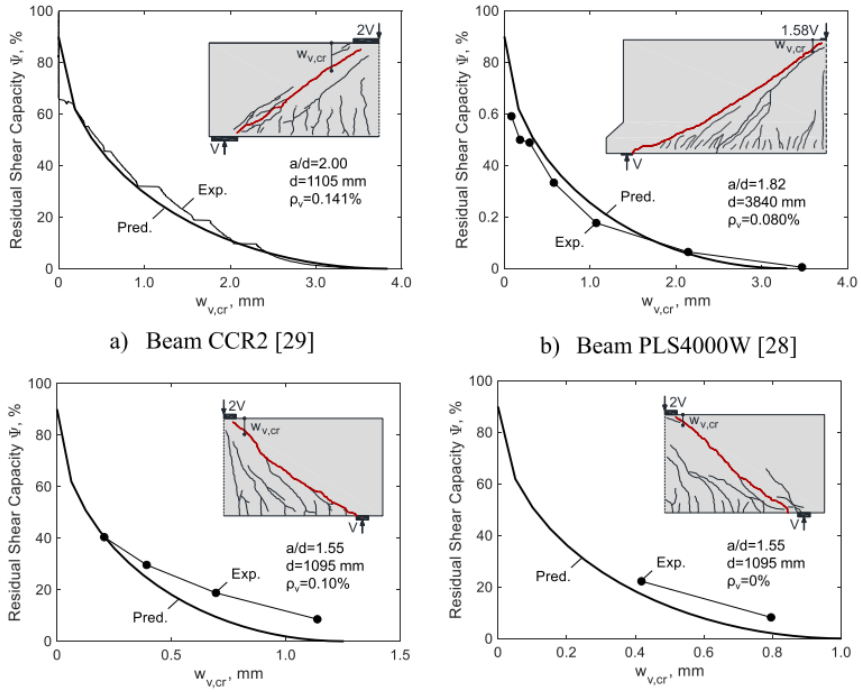

Figure 2.16: Measured and predicted residual shear capacity diagrams of specimens with variable properties [2].

2.2.4 Conclusion

The simplified and rapid crack-based assessment approach presented here allows to predict with a fairly good accuracy the residual shear capacity of deep beams based on only two simple closed-form equations together with three input parameters, which are represented by three measurements: the depth of the CLZ determined by the critical diagonal crack, the angle of the crack in the CLZ, and the critical vertical crack displacement at the edge of the CLZ.

Although this approach does not explicitly address long-term effects such as fatigue and creep, these are nevertheless implicitly taken into account. In fact, fatigue and creep have the effect of increasing the critical vertical crack displacement over time, resulting in a decrease

in the residual shear capacity of the beam. This model predicts this through the equation 2.22 which shows a decrease in ψ with $w_{v,cr}$.

As the critical vertical crack displacement is not recovered after unloading the beam, thus, the residual shear capacity predicted by this model shows the load closest to the failure load that the beam has experienced throughout its entire service life. This model would therefore allow long-term monitoring, by imposing a limit on the residual shear capacity of the beam, which decreases monotonically over time.

This rapid crack-based assessment approach therefore combines parsimony with high accuracy and explaining power.

Chapter 3

Simplified 2PKT Model for the Shear Strength of Deep Beams (ULS)

In this chapter, a simplified approach to the 2PKT model for predicting the shear strength of deep beams is presented.

The 2PKT model outlined in the preceding chapter is undoubtedly reasonably precise, however it necessitates a substantial amount of calculation. Firstly, the method is iterative. In equation 2.13, the expression for the maximum strain along bottom longitudinal reinforcement $\epsilon_{t,max}$ is a function of the shear strength of the beam V, which must be determined. Subsequently, the shear strength components are functions of several parameters whose expressions and calculation are rather cumbersome.

The aim of this simplified approach is therefore, on the basis of the full 2PKT model, to develop a non-iterative model whose shear strength component expressions are fairly simple closed-form design equations, like those for slender beams, while maintaining a good level of accuracy.

3.1 Formulation

3.1.1 Shear Resisted by The Critical Loading Zone V_{CLZ}

As shown in section 2.1.2, the critical loading zone (CLZ) is an important component of the 2PKT model. Based on the idealized geometry of this zone, its shear strength is given by :

$$V_{CLZ} = k f_{avg} b l_{b1e} \sin^2 \alpha \tag{3.1}$$

Based on physical assumptions, this expression can be further simplified.

3.1.1.1 Effective width of loading plate l_{b1e}

l_{b1e} represents the effective width of loading plate parallel to longitudinal axis of member. In the full 2PKT model, it is expressed as :

$$l_{b1e} = max[(V/P)l_{b1}, 3a_g] \tag{3.2}$$

In most cases, the effective width of the loading plate l_{b1e} is not less than three times the maximum size of coarse aggregate a_g. So :

$$l_{b1e} \approx (V/P) l_{b1} \tag{3.3}$$

V/P represents the fraction of the total applied load carried by the shear span studied. This fraction can be determined by the equilibrium equations, without needing to know V. For a beam on two supports loaded at mid-span, $V/P = 0.5$; for a beam on two supports taking two point loads P applied symmetrically about the centre of the beam, $V/P = 1$; and so on.

3.1.1.2 Angle α

The angle α represents the angle of line extending from inner edge of support plate to far edge of tributary area of loading plate responsible for shear force V. In the full 2PKT model, its tangent is expressed by :

$$\tan\alpha = \frac{h}{a - l_{b1}/2 - l_{b2}/2 - l_{b1e}} \tag{3.4}$$

In reality, the supports and loading points of deep beams are usually columns with approximately the same width, which is expressed by $l_{b1} = l_{b2}$. Thus, the term $(l_{b1}/2 + l_{b2}/2 + l_{b1e} \approx l_{b1} + l_{b1e})$ is generally negligible compared to the beam shear span a. The expression for the tangent of angle α thus becomes

$$\tan\alpha \approx \frac{h}{a} \rightarrow \alpha \approx \arctan(\frac{h}{a}) \tag{3.5}$$

As seen above in the full 2PKT model, k is a crack shape coefficient which equals 1 for beams with $\cot\alpha \leq 2$ and 0 for those with $\cot\alpha \geq 2.5$, with a linear transition for intermediate values of $\cot\alpha$. Thus :

$$k = min[max(5 - 2\cot\alpha, 0), 1] \tag{3.6}$$

By replacing parameters of equation 3.1 by their expressions, V_{CLZ} is finally given by the equation :

$$V_{CLZ} = min[max(5 - 2\cot\alpha, 0), 1] f_{avg} b (V/P) l_{b1} \sin^2\alpha \tag{3.7}$$

3.1.2 Shear Resisted by Aggregate Interlock V_{ci}

Aggregate interlock represents the second largest component of the shear resistance of deep beams after V_{CLZ} in most cases. It is due to the slip displacement of the critical diagonal crack which generates large shear stresses. In the full 2PKT model, the shear taken up by the aggregate interlock is expressed by :

$$V_{ci} = \frac{0.18\sqrt{f'_c}}{0.31 + \frac{24w}{a_{ge}+16}} bd \tag{3.8}$$

As shown in equation 3.8, this component depends on the width of the critical diagonal crack at failure w. Thus, simplifying this expression requires simplifying the formulation of w, while remaining conservative because the resistance provided by aggregate interlock decreases with the width of the crack.

3.1.2.1 Width of critical diagonal cracks

In the full 2PKT model, the width at failure of critical diagonal cracks is predicted at the mid-depth of the member by :

$$w = \Delta_c \cos\alpha_1 + \frac{\epsilon_{t,min} l_k}{2 \sin\alpha_1} \tag{3.9}$$

The first term of this equation represents the contribution of the first degree of freedom to this width and the second term the contribution of the second degree of freedom.

The iterative nature of the method comes from the minimum strain along bottom longitudinal reinforcement $\epsilon_{t,min}$ which depends on the shear strength V to be determined, as shown in equation 2.13. So, in order to develop a non-iterative approach, we need to make the determination of $\epsilon_{t,min}$ non-iterative.

3.1.2.1.1 Minimum strain along bottom longitudinal reinforcement $\epsilon_{t,min}$

In the full iterative model, minimum strain along bottom longitudinal reinforcement is expressed as :

$$\epsilon_{t,min} \approx \epsilon_{t,max} = \frac{T_{max}}{E_s A_s} = \frac{Va}{E_s A_s (0.9d)} \tag{3.10}$$

In practice, a beam is firstly designed for bending in the majority of cases. The bottom longitudinal reinforcement is sized to carry the maximum bending moment. Thus :

$$\epsilon_{t,max} = \frac{M_{Ed}}{E_s A_s (0.9d)} \tag{3.11}$$

where M_{Ed} is the maximum applied bending moment. By designing for bending, $M_{Ed} = M_{Rd}$, the resistant bending moment. Thus, the minimum strain along bottom longitudinal reinforcement can be approximated by :

$$\epsilon_{t,min} \approx \epsilon_{t,max} = \frac{M_{Rd}}{E_s A_s (0.9d)} \tag{3.12}$$

$$= \frac{f_y A_s (0.9d)}{E_s A_s (0.9d)} \tag{3.13}$$

$$= \frac{f_y}{E_s} \tag{3.14}$$

so

$$\epsilon_{t,min} \approx \epsilon_{t,max} = \frac{f_y}{E_s} = \epsilon_y \tag{3.15}$$

The expression of the minimum and maximum strain along bottom longitudinal reinforcement is therefore no longer iterative, and is safe because in the case of deep beams, they very rarely reach ϵ_y at shear failure.

The other parameters in the expression of w are determined in a non-iterative way but still require simplifications in order to obtain a relatively simple closed-form equation for V_{ci}.

3.1.2.1.2 Ultimate shear displacement Δ_c

The ultimate shear displacement is expressed as in equation 2.9 by :

$$\Delta_c = 0.0105 l_{b1e} \cos\alpha \tag{3.16}$$

By replacing l_{b1e} by its simplified expression at equation 3.3

$$\Delta_c = 0.0105 (V/P) l_{b1} \cos\alpha \tag{3.17}$$

3.1.2.1.3 Angle of the critical diagonal crack α_1

As the ratio a/d increases, the critical diagonal crack flattens, with the minimum required value θ which is the angle of diagonal cracks in uniform stress field. However, deep beams extend up to a ratio a/d of the order of 2.3, and the diagonal crack therefore generally develops between the loading point and the support in the critical shear span. As mentioned above, in practice, the loading points and supports are generally columns of relatively small widths compared to the height of the beam. Thus, the angle of the critical diagonal crack can be approximated by :

$$\alpha_1 = max[\alpha, \theta] = \alpha \tag{3.18}$$

3.1.2.1.4 Length of dowels l_k

As seen in equation 2.5, l_k represents the length of the longitudinal bottom reinforcement whose elongation contributes to the width of the critical crack, and is expressed in the full model as

$$l_k = l_0 + d(\cot\alpha - \cot\alpha_1) \tag{3.19}$$

Following the assumption made above that $\alpha_1 = \alpha$ in most cases:

$$l_k = l_0 \tag{3.20}$$

l_0 can then be simplified with the following expression :

$$l_0 = 1.5(h-d)\cot\alpha \tag{3.21}$$

In fact, the quantity $1.5(h-d)$ represents approximately the depth of the zone directly outside the crack control. l_0 is therefore the projection of the depth this zone onto the horizontal, which represents the length of the heavily cracked zone at the bottom of the critical crack.

By replacing the non-iterative formulation of $\epsilon_{t,min}$ and the simplified expressions of the other parameters in the formulation of w in equation 3.9, the result is :

$$w = \Delta_c \cos\alpha + \epsilon_y \frac{1.5(h-d)\cot\alpha}{2\sin\alpha} \tag{3.22}$$

This equation giving the critical diagonal crack width is non-iterative. It remains fairly conservative, mainly in its second term as presented here, but also fairly precise, as we will see later.

Based on this formulation of w, V_{ci} is expressed as follows:

$$V_{ci} = \frac{0.18\sqrt{f'_c}}{0.31 + 24\frac{0.0105(V/P)l_{b1}\cos^2\alpha + 0.75\epsilon_y(h-d)}{(a_g+16)\sin\alpha}} bd \tag{3.23}$$

with a_g the maximum size of coarse aggregate, which is an approximated value of the effective size of coarse aggregate a_{ge}.

Through the closed-form equation 3.23, the shear resisted by the aggregate interlock is therefore determined in a non-iterative way, which considerably reduces the computing time of this simplified approach, compared to the full 2PKT approach.

3.1.3 Shear Resisted by Stirrups V_s

The shear carried by the transverse reinforcement (stirrups) is expressed in the full model as :

$$V_s = \rho_s b(d\cot\alpha_1 - l_0 - 1.5l_{b1e})f_v \tag{3.24}$$

The calculation of this component is certainly not iterative, but it is not direct either. It requires the calculations of f_v in equation 2.15 and ϵ_v in equation 2.16. The aim of simplifying the expression of this component is to obtain a closed-form equation like that giving V_s in the case of slender beams.

3.1.3.1 Stress in the stirrups at shear failure f_v

In the full 2PKT model, The stress in the stirrups at shear failure is given by :

$$f_v = E_s\epsilon_v \leq f_{yv} \tag{3.25}$$

It will be assumed that stirrups are designed for shear failure as is the case for slender beams, and as is generally the case for deep beams too. This assumption allows to dispense with calculations in equations 2.15 and 2.16, and thus to have :

$$f_v = f_{yv} \tag{3.26}$$

3.1.3.2 Working length of stirrups

In the full model, the length along the shear span within which the critical crack is wide enough to cause significant tension in the stirrups is expressed by :

$$d \cot \alpha_1 - l_0 - 1.5 l_{b1e} \tag{3.27}$$

For slender beams, this working length of the stirrups is approximated by :

$$0.9 d \cot \alpha \tag{3.28}$$

In order to have a similar expression deep beams, the expression 3.27 can be simplified by :

$$0.3 d \cot \alpha \tag{3.29}$$

This expression is justified by the order of magnitude of $l_0 + 1.5 l_{b1e}$ compared with $d \cot \alpha_1$.

By replacing the expression in brackets in equation 3.24 by the one in equation 3.29, and f_v by f_{yv}, the formulation of the shear resisted by stirrups in deep beams in this simplified approach of the 2PKT model is therefore given by :

$$V_s = \rho_s b (0.3 d \cot \alpha) f_{yv} \tag{3.30}$$

3.1.4 Shear Resisted by The Dowel Action V_d

The shear carried by the dowel action is expressed in the full model by :

$$V_d = n_b f_{ye} \frac{d_b^3}{3 l_k} \tag{3.31}$$

with the effective yield strength

$$f_{ye} = f_y [1 - (\frac{T_{min}}{f_y A_s})^2] \leq 500 [Mpa] \tag{3.32}$$

which accounts for the effect of the tension in the bars.

As seen in equation 3.15 which makes the computation of the minimum strain along bottom longitudinal reinforcement non-iterative, the assumption that the bending resistance uses all the capacity of the bottom longitudinal reinforcement is made. Thus,

$$T_{min} \approx T_{max} = f_y A_s \tag{3.33}$$

As a result, there would be no capacity left in the bottom longitudinal reinforcement for the dowel action, and therefore :

$$f_{ye} = f_y[1 - (\frac{T_{min}}{f_y A_s})^2] = f_y[1 - (\frac{f_y A_s}{f_y A_s})^2] = 0 \tag{3.34}$$

This results in a zero contribution to shear strength :

$$V_d = 0 \tag{3.35}$$

Thus, in this simplified approach of the 2PKT model, the shear resisted by the dowel action is zero and not taken into account. This simplification is still adequate however, as it compensates for the overestimation of the shear strength of deep beams introduced by the new expression for the minimum strain along bottom longitudinal reinforcement in equation 3.15.

3.1.5 Summary of Shear Strength Components

In summary, as a result of the simplification of the 2PKT model intended to make the determination of the shear strength of deep beams non-iterative through simple closed-form design equations, the shear strength components of deep beams are given by :

- The shear resisted by the critical loading zone :

$$V_{CLZ} = min[max(5 - 2\cot\alpha, 0), 1] f_{avg} b (V/P) l_{b1} \sin^2\alpha \tag{3.36}$$

- The shear resisted by the aggregate interlock :

$$V_{ci} = \frac{0.18\sqrt{f'_c}}{0.31 + 24\frac{0.0105(V/P)l_{b1}\cos^2\alpha + 0.75\epsilon_y(h-d)}{(a_g+16)\sin\alpha}} bd \tag{3.37}$$

- The shear resisted by the transverse reinforcement (stirrups) :

$$V_s = \rho_s b(0.3d\cot\alpha) f_{yv} \tag{3.38}$$

- The shear resisted by the dowel action :

$$V_d = 0 \tag{3.39}$$

with

- α the angle of line extending from inner edge of support plate to far edge of tributary area of loading plate responsible for shear force V :

$$\alpha = \arctan(\frac{h}{a}) \tag{3.40}$$

- $\epsilon_{t,min}$ the minimum strain along bottom longitudinal reinforcement :

$$\epsilon_{t,min} \approx \epsilon_{t,max} = \frac{f_y}{E_s} = \epsilon_y \tag{3.41}$$

- f_{avg} the average diagonal compressive stress in the CLZ :

$$f_{avg} \approx 1.43 f_c'^{0}.8 \tag{3.42}$$

The accuracy of these equations will then be presented through predictions of the shear failure behavior of deep beams made on a total of 327 published tests on simply supported beams with a/d between 0.5 and 2.5.

3.2 Test database

In order to verify the simplified approach of the two-parameter kinematic theory presented above, a total of 327 published tests on simply supported beams with a/d between 0.5 and 2.5 were used, for which data are given in the appendix. These beams and their data come from the database used for the verification of the two-parameter kinematic theory [1] which contains 529 specimens. This database has therefore been filtered beforehand for the verification of this simplified approach, as not all the specimens meet the conditions for the application of this approach.

In fact, the key component of the 2PKT is the critical loading zone (CLZ), which provides the greatest shear strength contribution in deep beams. Thus, the shear failure mode of the beam predicted by this model corresponds to the crushing shear failure of the critical loading zone (**2PKT mode = C**). Specimens in the initial database whose predicted shear failure mode differs from this have been excluded.

In order to subsequently compare the simplicity and accuracy of the full 2PKT model and the simplified one, specimens for which the ratio between the experimentally determined shear strength and that predicted by the 2PKT method was not given in the initial database were also excluded.

Following these two conditions, there are 327 elements left in this database for which this simplified approach is verified.

The data for these beams corresponds to : **geometric properties of members and supports, reinforcement details, material properties, force data, failure modes predicted by different approaches, and the ratio of experimentally observed shear strength to that predicted by each approach**.

3.3 Validation

On the basis of the database presented above, the simplified approach of the two-parameter kinematic theory developed in this work has been verified and validated.

3.3.1 Validation of the Full 2PKT Model against Experimental Tests

In order to fully validate the simplified approach of the two-parameter kinematic theory , it is first necessary to validate the full model against experimental tests based on predictions made on the specimens in the filtered database.

In fact, The 2PKT approach developed here is a simplification of the full model. The accuracy of this model should therefore be checked beforehand by comparing the results obtained using it with those following experimental tests, which are closer to the reality.

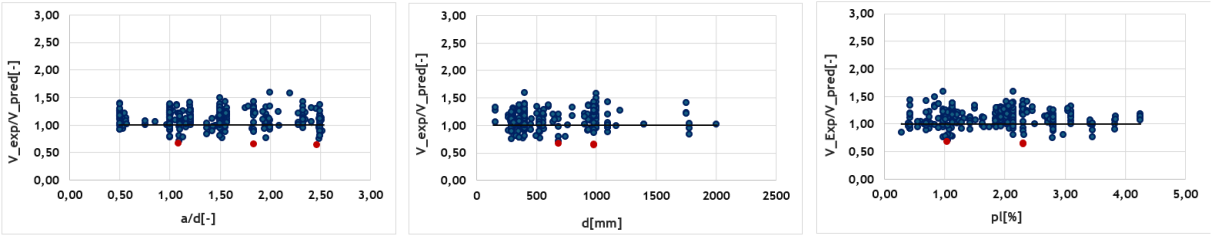

Figure 3.1: Comparison of 2PKT predictions with experimental observations for 327 tests.

The average ratio of experimental to predicted shear strengths for these tests is 1.11 with a coefficient of variation of 13.72%.

As shown in Figure 3.1, the full 2PKT model gives fairly accurate predictions, with a coefficient of variation of 13.72%. This model is also fairly conservative, as can be seen in figure 3.1. The ratios of experimental to predicted shear strengths are for the most part ≥ 1 (261 specimens in total, i.e. 80% of the test specimens) with an average of 1.11, which means that in general the real shear strength of the deep beam is underestimated using this model.

One of the main motivations for developing the 2PKT model was to take better account of size effect in deep beams. Figure 3.1 shows that this is indeed the case, given the small dispersion relative to 1 of the ratios for deep beams with large spans ($d > 1500mm$).

So, based on this filtered database of 327 specimens, the accuracy of the 2PKT model was found to be adequate, given the complexity of an accurate prediction of the shear strength of a deep beam.

3.3.2 Validation of the Simplified 2PKT Model against the Full 2PKT Model

Having validated the full 2PKT model against experimental tests, it is now necessary to validate the simplified approach of this model against the full one.

Indeed, the model developed during this work results from a simplification of the two-parameter kinematic theory as presented above in section 3.1, which aims to make the initially iterative 2PKT method non-iterative, and to define simple closed-form design equations against shear failure for deep beams, as is the case for slender beams.

As in the previous section, therefore, the accuracy of this simplified model must be checked against the full one.

3.3.2.1 Minimum strain along bottom longitudinal reinforcement $\epsilon_{t,min}$

In the full 2PKT model, the minimum strain along bottom longitudinal reinforcement is given by :

$$\epsilon_{t,min} = \frac{Va}{E_s A_s (0.9d)} \tag{3.43}$$

As explained above, the computation of the latter is iterative since it depends on the shear strength of the deep beam V which is the unknown to be determined. This is where the iterative nature of the initial 2PKT model comes from. In order to make this model non-iterative and direct, this expression of $\epsilon_{t,min}$ is approximated by :

$$\epsilon_{t,min} = \frac{f_y}{E_s} = \epsilon_y \tag{3.44}$$

To assess the accuracy of this simplification, the ratio between $\epsilon_{t,min}$ predicted by the full approach (equation 3.10) and that predicted by the simplified approach (equation 3.14) is calculated for each of the 327 specimens in the database.

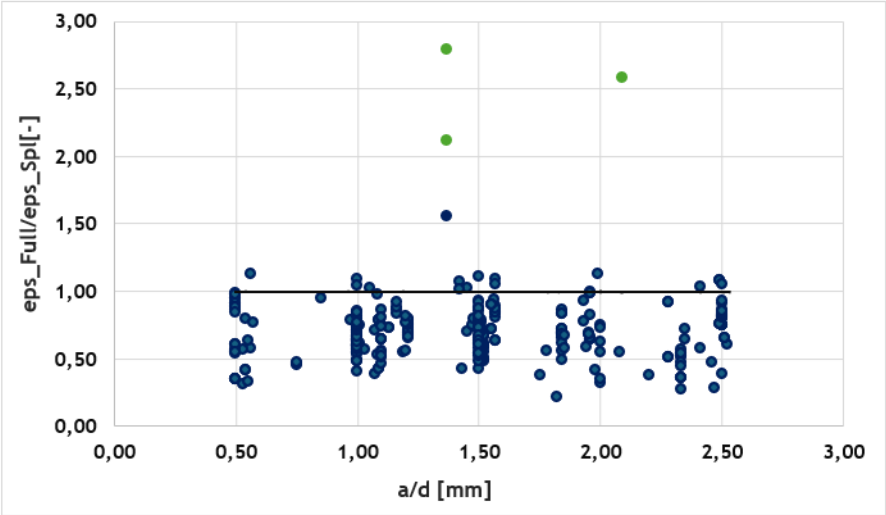

Figure 3.2: Predictions of Full vs Simplified 2PKT model for $\epsilon_{t,min}$.

The average ratio of full 2PKT to simplified 2PKT minimum strains along bottom longitudinal reinforcement for these tests is 0.71 with a coefficient of variation of 35.46%.

As shown in Figure 3.2 and as expected, the minimum strain along bottom longitudinal reinforcement is overestimated by approximating $\epsilon_{t,min}$ by ϵ_y, with a coefficient of variation of 35.46% which is quite high.

However, $\epsilon_{t,min}$ is a parameter in the expression of the critical diagonal crack width w, so we need to assess the influence of its simplification on w.

3.3.2.2 Width of critical diagonal cracks

The width of critical diagonal cracks is expressed in the full 2PKT model as :

$$w = \Delta_c \cos\alpha_1 + \frac{\epsilon_{t,min} l_k}{2 \sin\alpha_1} \tag{3.45}$$

In the simplified approach, it is expressed as :

$$w = \Delta_c \cos\alpha + \epsilon_y \frac{1.5(h-d)\cot\alpha}{2\sin\alpha} \tag{3.46}$$

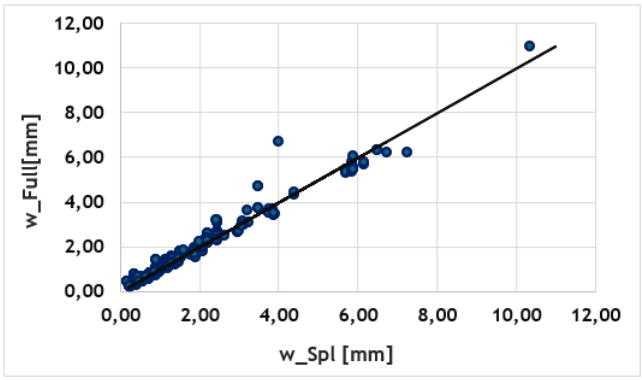

(a) Predictions of full vs simplified 2PKT model for w.

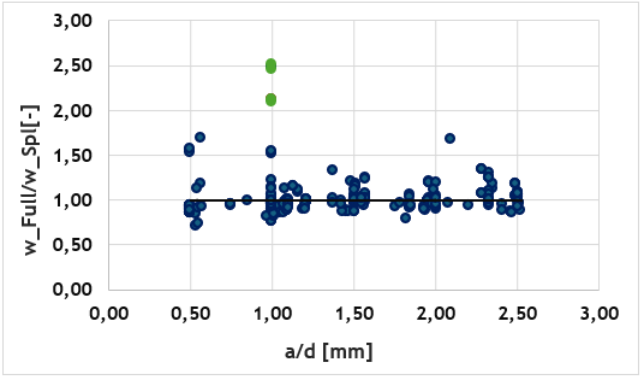

(b) Ratio of full to simplified 2PKT predictions for w.

Figure 3.3: Predictions of Full vs Simplified 2PKT model for w.

The average ratio of full to simplified 2PKT predictions of crack widths for these tests is 1.03 with a coefficient of variation of 21.03%.

As shown in Figure 3.3(a), the crack width predictions through the simplified approach match quite well with those through the full approach. There is less scatter around 1 in the crack width ratios calculated through these two models as shown in Figure 3.3(b), in contrast to previously in Figure 3.2.

Indeed, the overestimation of the minimum strain along bottom longitudinal reinforcement $\epsilon_{t,min}$ following its simplification is counterbalanced in the end in w mainly in the approximation of l_k by $1.5(h-d)\cot\alpha$ which reduces the contribution of the second degree of freedom on the crack width. For some specimens, the length of dowels provided by bottom longitudinal reinforcement l_k is greater than $1.5(h-d)\cot\alpha$. Thus, for some specimens specimens, $\epsilon_{t,min}$ is overestimated and l_k is underestimated, which attenuates the impact of the simplifications on the second term of w, the first term relating to the first degree of freedom already being little influenced.

The width of critical diagonal cracks w is indirectly related to the shear strength of the deep beam V through its component V_{ci}, the shear resisted by aggregate interlock.

3.3.2.3 Shear resisted by aggregate interlock V_{ci}

The shear carried by aggregate interlock is expressed in the full 2PKT model by:

$$V_{ci} = \frac{0.18\sqrt{f'_c}}{0.31 + \frac{24w}{a_{ge}+16}} bd \tag{3.47}$$

with w presented in the equation 3.9. In the simplied approach, it is expressed by :

$$V_{ci} = \frac{0.18\sqrt{f'_c}}{0.31 + 24\frac{0.0105(V/P)l_{b1}\cos^2\alpha + 0.75\epsilon_y(h-d)}{(a_g+16)\sin\alpha}} bd \tag{3.48}$$

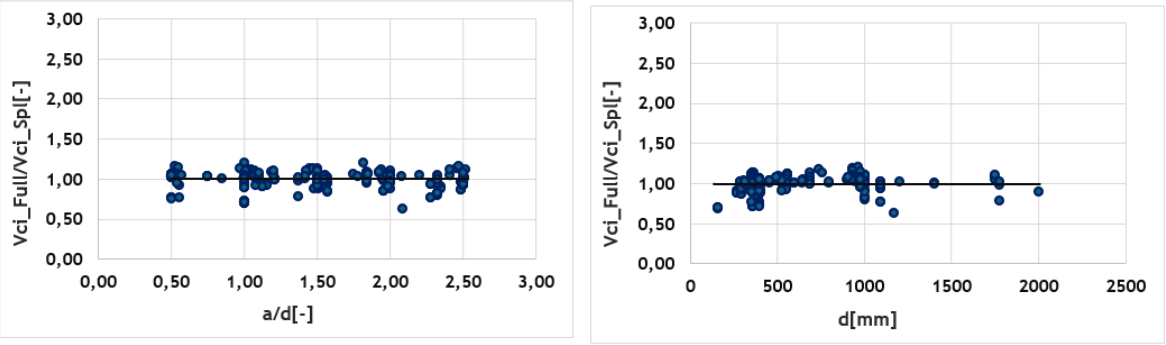

Figure 3.4: Predictions of Full and Simplified 2PKT model for V_{ci}.

The average ratio of full to simplified 2PKT predictions of V_{ci} for these tests is 0.99 with a coefficient of variation of 8.79%.

As shown in Figure 3.4, by switching from an iterative to a direct determination of aggregate interlock shear strength, we nevertheless retain fairly good accuracy. The coefficient of variation of ratios of V_{ci} predicted by the full 2PKT model to that predicted by the simplified approach is 8.79%, much lower than the previous one concerning w which is 21.03%.

The effect of simplifications made to the width of critical cracks w on one hand through $\epsilon_{t,min}$ by making its determination direct and on the other hand through the other parameters such as α_1 and l_k is further attenuated in V_{ci}.

Predictions of the shear strength component V_{ci} are therefore still fairly accurate, which shows that assumptions made for its simplification which already make physical sense, are also acceptable.

3.3.2.4 Shear resisted by the critical loading zone V_{CLZ}

The critical loading zone is a key component of the 2PKT model. It is the one of the four components that makes the greatest contribution to the shear strength of the deep beam. In the full 2PKT model, it is expressed as :

$$V_{CLZ} = k f_{avg} b l_{b1e} \sin^2\alpha \tag{3.49}$$

with l_{b1e} and α expressed in equations 3.2 and 3.4 respectively. In the simplified model, it is expressed by :

$$V_{CLZ} = min[max(5 - 2\cot\alpha, 0), 1] f_{avg} b (V/P) l_{b1} \sin^2\alpha \tag{3.50}$$

with $\alpha = \arctan(\frac{h}{a})$.

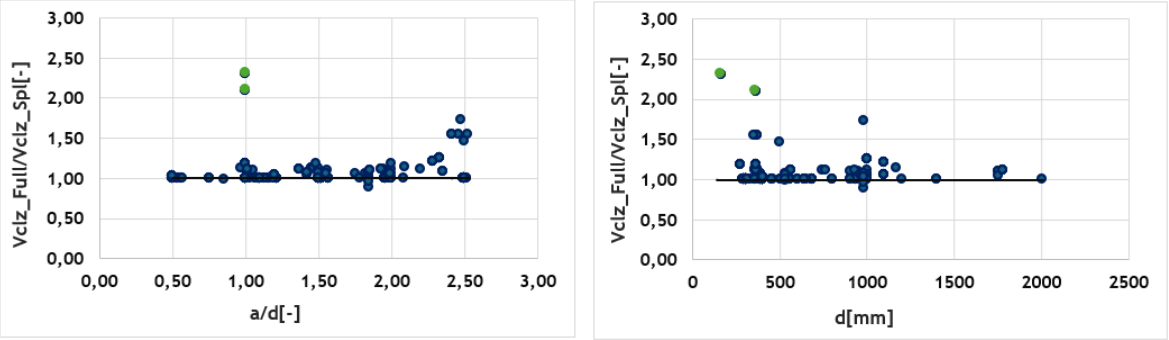

Figure 3.5: Predictions of Full and Simplified 2PKT model for V_{CLZ}.

The average ratio of full to simplified 2PKT predictions of V_{CLZ} for these tests is 1.07 with a coefficient of variation of 17.30%.

As shown in Figure 3.5, the accuracy of the prediction of V_{CLZ} in the simplified approach remains fairly good, with a coefficient of variation of ratios of V_{CLZ} predicted by the full method to that predicted by the simplified method of 17.30%.

Indeed, for the 327 specimens in the database, the shear resisted by the critical loading zone represents on average 60% of the total shear strength of the deep beam following the full 2PKT model. It therefore represents the most important component as mentioned above. This is why simplifications made to it in the simplified approach were not performed to reduce the predicted values of V_{CLZ} for most specimens.

It is therefore necessary to remain conservative in the prediction of V_{CLZ} in order to remain conservative in the prediction of the shear strength of the deep beam, as shown in figure 3.5 with an average contribution of the CLZ on the shear strength of the deep beam of 64%. This average contribution is larger in the simplified approach of the 2PKT model in order to account for the fact that the shear resisted by the dowel action is neglected.

3.3.2.5 Shear strength of the deep beam

In the full 2PKT model, the shear strength of the deep beam is given by :

$$V = V_{CLZ} + V_{ci} + V_s + V_d \tag{3.51}$$

It is calculated iteratively. In the simplified approach developed, the shear strength is calculated directly, i.e. non-iteratively, and is expressed by :

$$V = V_{CLZ} + V_{ci} + V_s \tag{3.52}$$

with the components V_{CLZ}, V_{ci} and V_s calculated respectively through closed-form equations 3.7, 3.23 and 3.30.

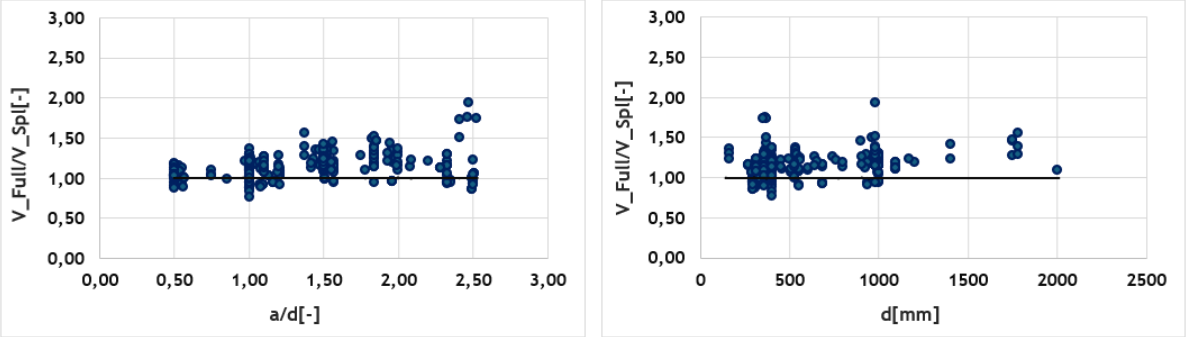

Figure 3.6: Predictions of Full and Simplified 2PKT model for the shear strength V.

The average ratio of full to simplified 2PKT predictions of V for these tests is 1.13 with a coefficient of variation of 13.79%.

As shown in Figure 3.6, the prediction of the shear strength of the deep beam remains conservative compared to the full model.

The non-inclusion in this simplified approach of the V_d component, which represents on average approximately 10% of the shear strength predicted by the full model, is partly compensated by an overestimation of V_{CLZ}, as seen above.

Despite this security, the approximated model is still fairly accurate, resulting in a reasonable coefficient of variation of the ratios between V predicted by the full model and V predicted by the simplified model of 13.79%.

3.3.3 Validation of the Simplified 2PKT Model against Experimental Tests

Now that the simplified 2PKT model has been validated against the full model, we need to validate it against the experimental tests, which give the results closest to those observed in reality.

Figures 2.3 and 3.3(a) show the same shape. Figure 2.3 shows good matching between the crack width predicted by the 2PKT model and that obtained experimentally, as does Figure 3.3(a) between the crack width predicted by the simplified model and that predicted by the full one. This comparison shows that the simplified approach is fairly accurate in predicting crack widths compared with the experimental tests.

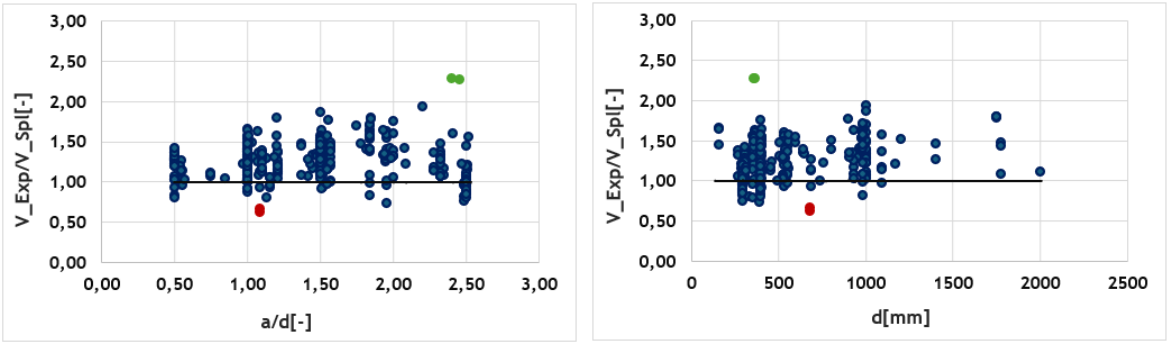

Figure 3.7: Experimental observations and predictions of the simplified 2PKT model for the shear strength V.

The average ratio of experimental to simplified 2PKT predictions of V for these 327 tests is 1.26 with a coefficient of variation of 18.81%.

As shown in Figure 3.7, the simplified approach developed in this work predicts the shear strength of a deep beam both conservatively and accurately. It is even more conservative for a/d between 0.5 and 2.3, which is the range of a/d for most deep beams.

Also, this simplified 2PKT model is even more accurate than the ACI and AASHTO models, which give coefficients of variation of the ratios between the shear strength obtained experimentally and that predicted of 24.6% and 29.0% respectively.

This simplified approach of the two-parameter kinematic theory allows the shear strength of a deep beam to be predicted conservatively and accurately using fairly simple closed-form shear design equations, as is the case for slender beams.

3.4 Discussion

The approach proposed in this work for the prediction of the shear strength of deep beams is based on the 2PKT model, which enables the beam's deformed shape to be predicted in terms of just of two degrees of freedom, and thus its shear resistance to be calculated knowing that, as is the case for slender beams. However, the prediction procedure presented in the 2PKT model is rather tedious to carry out, compared with that for slender beams. Indeed, the 2PKT method is firstly iterative, as the determination of the degree of freedom ϵ_{avg} which represents the average strain along bottom longitudinal reinforcement depends on the beam's shear strength V, which is precisely what is sought, as shown in equation 2.13. This therefore makes the method not direct and one of the shear design equations unclosed. Secondly, these design equations are rather cumbersome to implement, as they depend on several parameters that require prior calculations. Thus, the aim of the approach proposed here is to simplify the initial 2PKT model, by making it non-iterative, i.e. by making direct the determination of the degree of freedom $\epsilon_{t,avg}$, which is achieved through equation 3.15; and then by proposing closed-form shear design equations whose implementation requires almost no prior calculations. In other words, the aim of this approach is to propose a shear design procedure for deep beams similar to that for slender beams.

However, it is essential to maintain the accuracy of the results. Indeed, simplifying the initial model leads to a loss of precision, as the iterative calculation of $\epsilon_{t,avg}$ and the more

detailed expressions of other parameters make their estimates closer to the real values. The approach proposed here offers a fairly good compromise between simplicity and accuracy. It is validated on the basis of 327 published tests on simply supported beams, for which the coefficient of variation of ratios between the shear strength obtained experimentally and that predicted by the simplified model is 18.81% with an average ratio of 1.26, compared to the coefficient of variation of ratios with predictions through the full model of 13.72% with an average of 1.11. There is therefore a difference of 5.09% in the coefficients of variation, reflecting a slight loss of precision when switching to the simplified model. This loss of precision is nevertheless acceptable, given the simplicity provided by the new approach. It is therefore satisfactory.

One way to improve this new model would be a better account of the size effect. Indeed, a better understanding of the size effect is a key motivation of the development of the two parameter kinematic theory, and a comparison between figures 3.1 and 3.7 shows a reduction in its inclusion in the simplified model, with ratios that are more dispersed and shifted upwards from 1 for deep beams with large effective depth of section ($d > 1500mm$). So, taking a better account of this size effect would therefore lead to an increase in the accuracy of the new approach.

Chapter 4

Evaluation of Crack Widths in Deep Beams (SLS)

In this chapter, an approach for predicting the evolution of critical diagonal shear crack widths in deep beams during their service life is presented.

The model presented on a rapid crack-based assessment approach allows the residual shear capacity of deep beams to be predicted according to the current state of the beam, more precisely according to the current geometry of the critical diagonal shear crack located close to the point of loading, called the critical loading zone. However, at serviceability limit states, it is essential to be able to assess widths of these critical diagonal cracks in the beam. It is even more important to be able to do this in advance, i.e. before they appear, so that appropriate measures can be taken if necessary.

This is the aim of the model developed here: to predict fairly accurately the evolution of the shear crack width on a deep beam as a function of its loading. Indeed, it is still very difficult to accurately calculate the width of cracks on a deep beam. Therefore, in order to make the approach developed during this work as accurate as possible, it is based on the complete Two-Parameter Kinematic Theory (2PKT) presented in section 2.1, as well as on the Rapid Crack-Based Assessment approach (CBA) seen in section 2.2.

4.1 Formulation

In this work, two different formulations for crack width predictions following the applied shear are tested, with the main aim of improving the accuracy from the first formulation to the second.

4.1.1 Experimental observations

In order to verify each of the two formulations, predictions are made and compared with experimental results obtained on a test specimen named I-03-2.

4.1.1.1 Description of test I-03-2

An experimental study was carried out on test specimen I-03-2. This beam comes from a shear research project (Project 0-5253) carried out in Texas [3]. Figure 4.1 shows its

geometrical and material properties, the main ones being : a shear-span-to-effective-depth ratio $a/d = 1.84$; a flexural reinforcement ratio $\rho_l = 2.29\%$; and a transverse reinforcement ratio $\rho_v = 0.29\%$. All properties are listed in the appendix.

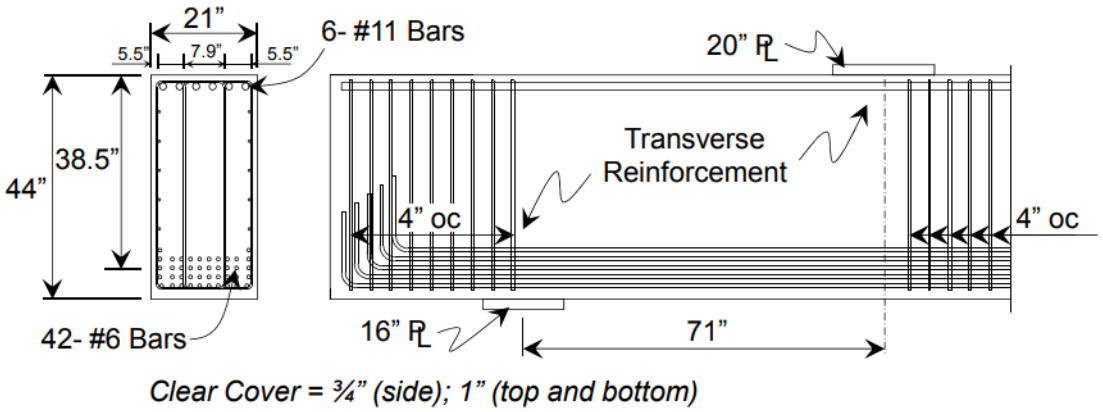

Figure 4.1: Beam geometry, reinforcement, and material properties of specimen I-03-2 [3].

Note : "oc" stands for "on center"; "P_L" represents the loading or support plate; and 1" = 25.4[mm].

The beam was subjected to an asymmetrical three-point bending test. Initially, the load was applied near one of the supports in accordance with the designated a/d ratio, and the behavior of the specimen was monitored until shear failure occurred in the corresponding test zone. After this failure, external post-tensioned clamps were installed to reinforce the damaged region. The hydraulic actuator was then repositioned to the opposite end of the beam, again based on the required a/d ratio, and the beam was reloaded. The behavior of this second test region was subsequently monitored. This process is illustrated in figure 4.2 below.

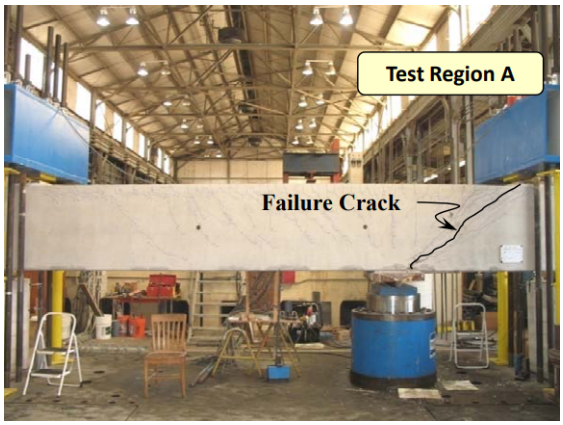

(a) Shear failure in Test Region A.

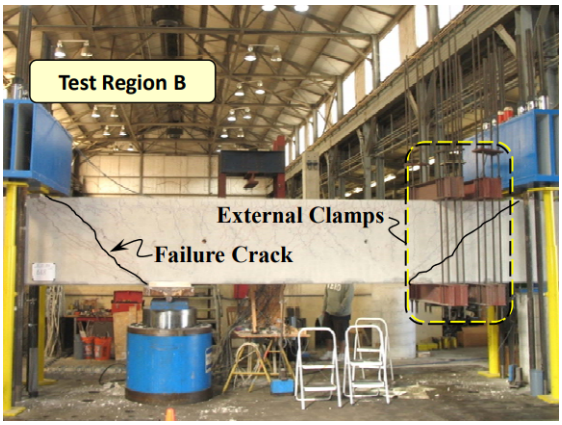

(b) Shear failure in Test Region B.

Figure 4.2: Loading process of the beam up to complete failure [3]].

In this way, the two shear spans are considered, since in reality the critical shear span is not known in advance. This also makes it possible to account for any random variability in the results obtained.

4.1.1.2 Observed behavior of specimen I-03-2

At each stage of loading a test region to failure, the width of each diagonal crack is recorded. During this process, no distinction is made between flexure-shear cracks or web-shear cracks. However, as the applied shear increases, the main diagonal crack becomes more distinct, and its maximum width is generally recorded at mid-depth of the beam. Figure 4.3 below shows the process of measuring and recording crack widths.

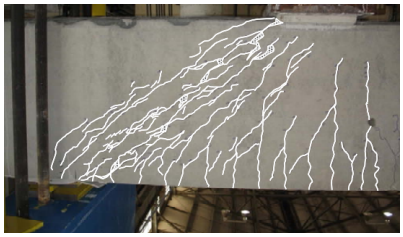

(a) Crack pattern at shear failure.

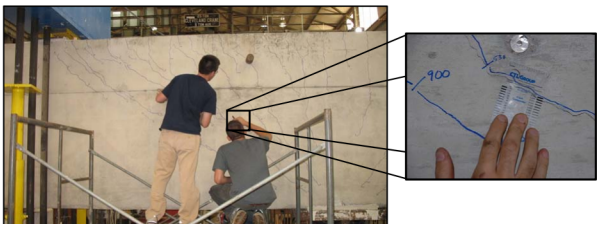

(b) Crack width measurement technique.

Figure 4.3: Recording of maximum diagonal crack width [3].

The table 4.1 below shows the maximum width of diagonal cracks observed in both regions at each loading stage.

$V/V_u[\%]$	$V[kN]$	$w_{Exp}[mm]$
0	0	0.00
15	380	0.00
23	582	0.15
33	835	0.33
43	1088	0.51
53	1341	0.64
63	1595	0.76
73	1848	0.89
83	2101	1.22
93	2354	1.52
100	2531	-

Table 4.1: Measured crack widths at all loading stages for specimen I-03-2 [4].

Therefore, figure 4.4 shows the evolution of the maximum width of diagonal cracks following the loading during the test.

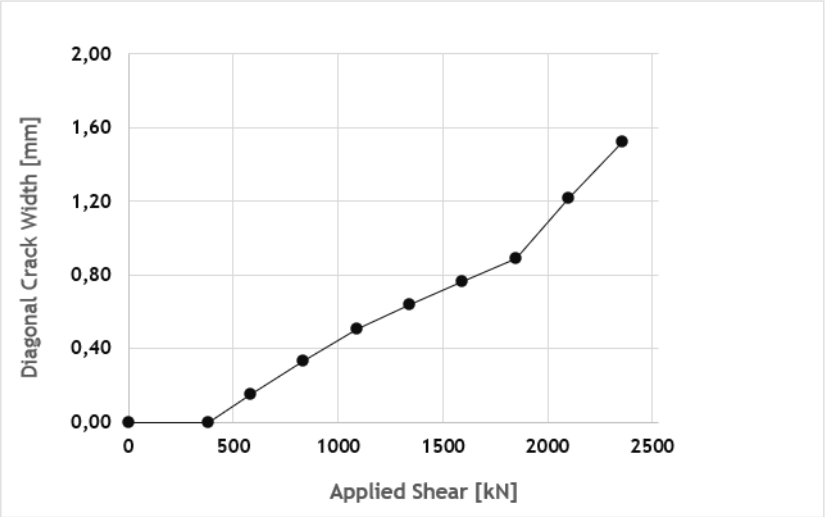

Figure 4.4: Evolution of measured crack width following the applied shear for specimen I-03-2.

The maximum width of diagonal cracks therefore increases with the applied shear, which is consistent with the physics of the problem. These experimental results are then compared with predictions of each of the two formulations developed.

4.1.2 First formulation

The first formulation is based explicitly on the expression of the width of critical diagonal cracks at mid-depth in the 2PKT model. It is expressed as seen in equation 2.5 by:

$$w = \Delta_c \cos \alpha_1 + \epsilon_{t,min} \frac{l_k}{2 \sin \alpha_1} \tag{4.1}$$

The first term of this equation represents the contribution to crack width from the first degree of freedom of the 2PKT model (the vertical shear displacement of the critical loading zone Δ_c) while the second term represents the contribution from its second degree of freedom (the average strain along bottom longitudinal reinforcement $\epsilon_{t,avg}$).

In order to predict the crack width as a function of the applied shear, i.e. to have an expression of the form $w(V)$, it is necessary to predict the vertical shear displacement of the critical loading zone as a function of the applied shear $\Delta_c(V)$ as well as the minimum strain along bottom longitudinal reinforcement $\epsilon_{t,min}(V)$.

4.1.2.1 Prediction of Δ_c as a function of V

As seen in the CBA approach presented in section 2.2 and more precisely by comparing figures 2.12 and 2.13, the vertical shear displacement of the critical loading zone Δ_c is nearly identical to the vertical crack displacement $w_{v,cr}$ due to the fact that the strains along bottom longitudinal reinforcement (the second degree of freedom $\epsilon_{t,avg}$) has a negligible influence on $w_{v,cr}$. Thus, at any load stage, Δ_c can be taken to be equal to $w_{v,cr}$. As shown in Figure 2.13a, the part of the width of the critical diagonal crack due to the degree of freedom Δ_c (whose vertical projection is in fact equals to Δ_c) is constant throughout the depth of the beam. Thus, the vertical displacement of the critical diagonal crack $w_{v,cr}$ can also be taken

as constant over the entire depth of the beam, and therefore as being the same at the edge of the CLZ and at the mid-depth of the beam.

A relationship between the vertical displacement of the critical diagonal crack $w_{v,cr}$ and the applied shear V is expressed in the residual shear capacity ψ in equation 2.22 :

$$\psi(w_{v,cr}) = (1 - \frac{V}{V_u}) * 100\% = 0.9[1 - \sqrt{1 - (1 - \frac{w_{v,cr}}{\Delta_{cu}})^2}] * 100\% \tag{4.2}$$

By rearranging this expression, $w_{v,cr}$ is expressed as a function of V by :

$$w_{v,cr} = \Delta_{cu}[1 - \sqrt{1 - \frac{1}{0.81}(\frac{V}{V_u} - 1)^2}] \tag{4.3}$$

Having shown that $w_{v,cr} \equiv \Delta_c$, it follows that :

$$\Delta_c = \Delta_{cu}[1 - \sqrt{1 - \frac{1}{0.81}(\frac{V}{V_u} - 1)^2}] \tag{4.4}$$

with V_u the shear strength of the deep beam and Δ_{cu} the ultimate vertical shear displacement of the critical loading zone expressed by :

$$\Delta_{cu} = 0.009 l_{b1e} \cot \alpha \tag{4.5}$$

This formulation of Δ_{cu} is obtained following equation 2.21, with the effective width of loading plate l_{b1e} presented in equation 3.2.

Equation 4.4 can therefore be used to predict the vertical shear displacement Δ_c as a function of V at each load stage during the service life of the beam.

4.1.2.2 Prediction of $\epsilon_{t,min}$ as a function of V

As shown in equation 2.13, the minimum strain along bottom longitudinal reinforcement is expressed in the 2PKT model as :

$$\epsilon_{t,min} \approx \epsilon_{t,max} = V \frac{a}{E_s A_s (0.9d)} \tag{4.6}$$

with a the shear span, d the effective depth of section and A_s the area of longitudinal bars on flexural tension side of section.

The equation 4.6 results simply from a rotational equilibrium at the most stressed section of the beam, and approximating the minimum strain along bottom longitudinal reinforcement $\epsilon_{t,min}$ by the maximum one $\epsilon_{t,max}$ introduces conservatism.

The equation 4.6 can therefore be used to predict the minimum strain along bottom longitudinal $\epsilon_{t,min}$ as a function of V at each load stage during the service life of the beam.

4.1.2.3 Expressions of α_1 and l_k

α_1 and l_k designate respectively the angle of critical diagonal crack and the length of dowels provided by bottom longitudinal reinforcement as shown in figure 2.2. In order to obtain the best accuracy, their expressions defined in the full 2PKT model are considered:

$$\alpha_1 = max[\alpha, \theta] \tag{4.7}$$

$$l_k = l_0 + d(\cot\alpha - \cot\alpha_1) \tag{4.8}$$

with

$$\alpha = \arctan(\frac{h}{a - l_{b1}/2 - l_{b2}/2 - l_{b1e}}) \tag{4.9}$$

$$\theta = 35.9^\circ \tag{4.10}$$

$$l_0 = 1.5(h-d)\cot\alpha_1 \geq s_{max} \tag{4.11}$$

$$s_{max} = \frac{0.28 d_b}{\rho_l}\frac{2.5(h-d)}{d} \tag{4.12}$$

4.1.2.4 Prediction of w as a function of V

Based on the predictions of the vertical shear displacement of the critical loading zone Δ_c and the minimum strain along bottom longitudinal reinforcement $\epsilon_{t,min}$, the width of the critical diagonal shear crack w can be therefore predicted as a function of the applied shear V at each load stage.

$$w(V) = \Delta_c(V)\cdot\cos\alpha_1 + \epsilon_{t,min}(V)\cdot\frac{l_k}{2\sin\alpha_1} \tag{4.13}$$

$$\Delta_c(V) = \Delta_{cu}[1 - \sqrt{1 - \frac{1}{0.81}(\frac{V}{V_u} - 1)^2}] \tag{4.14}$$

$$\epsilon_{t,min}(V) = V\frac{a}{E_s A_s(0.9d)} \tag{4.15}$$

4.1.2.5 Measured vs predicted response of specimen I-03-2

Firstly, in order to verify and validate or not the above formulation of the prediction of the width of the critical shear crack as a function of the applied shear V, a comparison is made between the results obtained experimentally (section 4.1.1) and those predicted by equation 4.13 on specimen I-03-2.

Thus, the table below shows the measured and the predicted widths of the main diagonal crack, respectively w_{Exp} and w_{Pred}, at different levels of the applied shear.

$V/V_u[\%]$	$V[kN]$	$w_{Exp}[mm]$	$w_{Pred}[mm]$
0	0	0.00	0.00
15	380	0.00	0.13
23	582	0.15	0.22
33	835	0.33	0.39
43	1088	0.51	0.60
53	1341	0.64	0.87
63	1595	0.76	1.21
73	1848	0.89	1.64
83	2101	1.22	2.20
93	2354	1.52	3.01
100	2531	-	3.94

Table 4.2: Measured and predicted crack widths at each loading stage for specimen I-03-2.

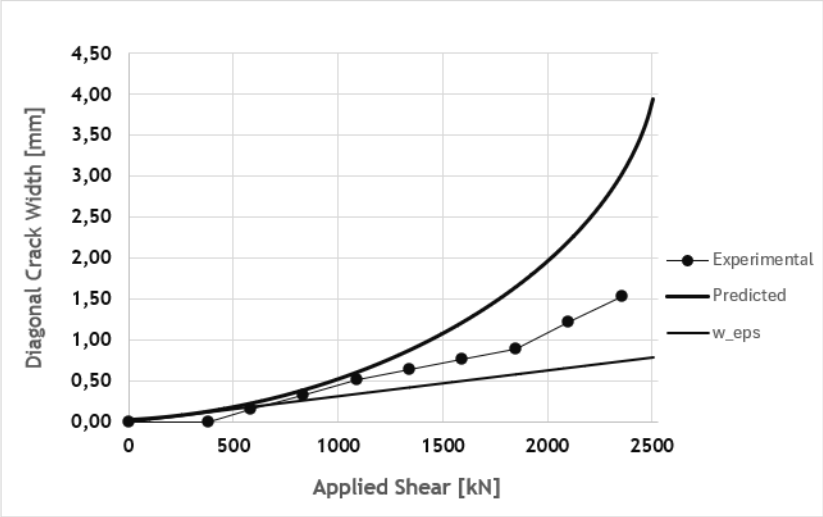

Figure 4.5: Measured and predicted crack widths for specimen I-03-2.

Figure 4.5 shows the predicted width of the critical diagonal shear crack at each loading stage of the beam.

This prediction is very conservative and rather overestimates the width of the crack, especially at high loads. In fact, the 'w_{-eps}' curve represents the contribution to the crack width from the bottom longitudinal reinforcement , i.e. the second term of the equation 4.13. This curve fits well with the first experimental measurements, since the first cracks to appear on the beam during loading are flexural cracks, which are therefore mainly due to the tension of the bottom longitudinal reinforcement. However, as the applied shear increases, there is a mismatch between the predictions and the measurements, which is mainly due to the contribution of the vertical shear displacement of the CLZ, i.e. the first term of equation 4.13.

This first formulation of the predicted shear crack width on a deep beam therefore mainly underestimates the restriction to the vertical displacement of the main crack $w_{v,cr} \equiv \Delta_c$. Other phenomena induced by the appearance of a main diagonal crack in a deep beam during its loading must be taken into account.

4.1.3 Second formulation

The previous formulation for predicting the width of the diagonal shear crack gives results that are certainly conservative, since it predicts crack widths greater than those obtained experimentally, but that are not sufficiently accurate. In fact, as the applied shear increases, the predicted crack width is greater than that measured, by a ratio of 2 approximately ($w_{Exp}/w_{Pred} \approx 0.5$).

In fact, the previous formulation does not incorporate the crack control effect that develops following the appearance of the critical diagonal crack and restricts its widening.

4.1.3.1 Crack control effect

Crack control is produced by the appearance of secondary cracks on either side of the critical diagonal crack.

Indeed, after the appearance of the critical diagonal crack at low load, other smaller cracks can develop above and below this main crack, which has the effect of distributing the loss of stiffness due to the cracking of the beam between the main crack and the secondary cracks, and therefore of slowing down the widening of the main crack when the load increases. This effect is all the more pronounced when the beam has web reinforcement because these force the appearance of secondary cracks. This is shown in figure 4.6 below, where for two beams almost identical at all points and varying only by the amount of web reinforcement, the one with web reinforcement shows several secondary cracks at approximately 100% of its shear capacity, while the one without web reinforcement shows very few at the same percent of applied shear. A more detailed comparative study of these two test specimens is carried out in section 4.3.1.

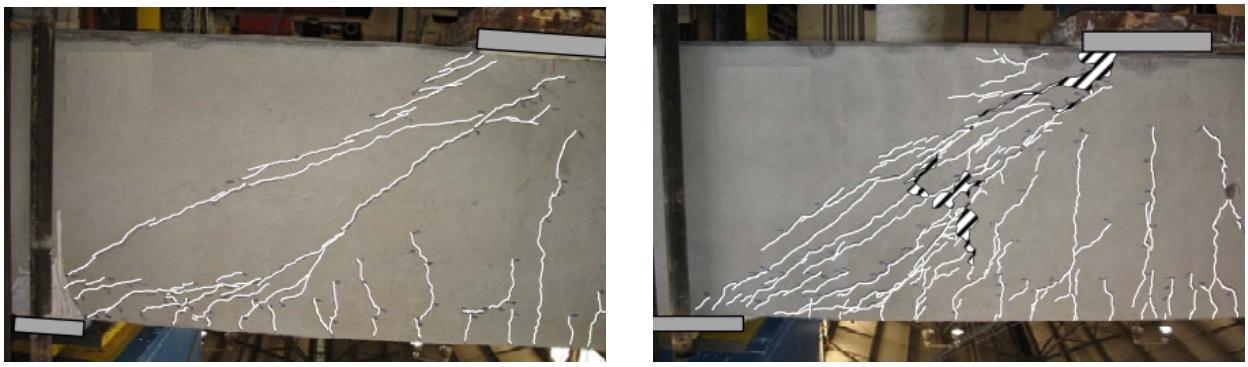

(a) Test III-1.85-00. (b) Test III-1.85-03b

Figure 4.6: Crack patterns in a specimen without (left) and with (right) web reinforcement at shear failure [3].

Thus, depending on the amount of web reinforcement and on the tensile strength of the concrete, secondary cracks inducing a crack control effect may or may not be taken into account.

4.1.3.2 Prediction of secondary cracks

The formation of secondary cracks first requires the presence of transverse reinforcement. The main diagonal crack widens as the stirrups progressively elongate. It is therefore assumed that secondary cracks do not appear until the stirrups are fully yielded. In other words, secondary cracks only develop when the width of the main crack w is equivalent to that due to yielding of the stirrups w_{vy}. The vertical crack width corresponding to yielding of the transverse reinforcement is expressed as follows:

$$w_{vy} = \frac{d_{bv} f_{yv}^2}{4\tau_b E_s} \tag{4.16}$$

$$\tau_b = 2f_{ct} \approx 2 * 0.33\sqrt{f_c} \tag{4.17}$$

with d_{bv} the diameter of stirrups, f_{yv} the yield strength of stirrups, f_{ct} the tensile strength of the concrete and τ_b the bond strength of stirrups. w_{vy} is obtained by integrating the strain profile along the transverse reinforcement at yielding.

As the crack displacement is nearly vertical, it is assumed that when the width of the critical diagonal crack w reaches w_{vy}, secondary cracks may appear on either side of it. In fact, in the vicinity of the main crack, aggregate interlock generates stresses that put the concrete in tension on either side of the main crack. Thus, at $w = w_{vy}$, according to the free-body diagram in figure 4.7, the total tensile stress induced at the main crack is expressed by :

$$f = v_{ci} \tan\alpha_1 + f_{yv}\rho_v \cos^2\alpha_1 + f_{yh}\rho_h \sin^2\alpha_1 \tag{4.18}$$

$$v_{ci} = \frac{0.18\sqrt{f'_c}}{0.31 + \frac{24 w_{vy}}{a_g + 16}} \tag{4.19}$$

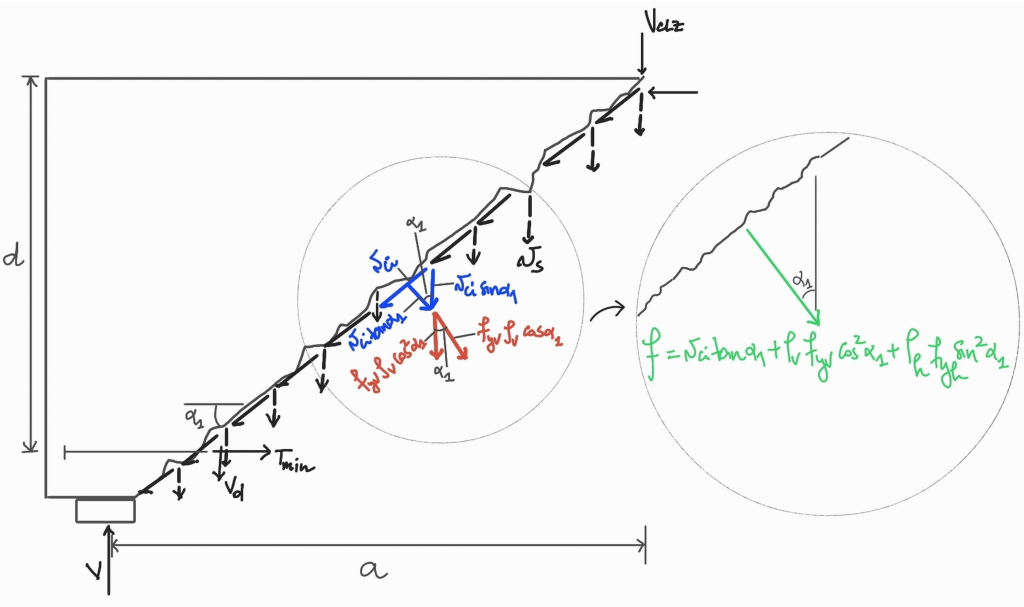

Figure 4.7: Tensile stress components within the critical diagonal shear crack.

The first term of equation 4.18 represents the tensile stress induced by aggregate interlock, the second term represents the maximum tensile stress induced by the transverse reinforcement and the last term represents the maximum tensile stress induced by the horizontal reinforcement. The expression for the tensile stress induced by aggregate interlock in equation 4.19 is taken from the 2PKT model (equation 2.12).

Thus, when this tensile stress is greater than the tensile strength of the concrete ($f \geq f_{ct}$), secondary cracks form on either side of the main crack and the total additional widening that would apply solely to this main crack is now distributed between it and the secondary cracks.

4.1.3.3 Prediction of w as a function of V

The width of the critical diagonal shear crack can then be predicted at each loading step. The second formulation of the prediction of w as a function of the applied shear V takes the first formulation developed in section 4.1.2 and includes the crack control effect to improve the accuracy of the results.

In fact, for a deep beam with web reinforcement, if the total tensile stress f induced at the vicinity of the main crack by aggregate interlock and by the yielding of the web reinforcement exceeds the tensile strength of the concrete f_{ct}, secondary cracks form when the width of the main crack w reaches that due to the yielding of the stirrups w_{vy}, and therefore the additional widening is distributed between the secondary cracks and the main crack. The secondary cracks on each side of the main crack can be combined to form a single crack. Thus, the idealised cracking pattern of the beam considers three cracks: a diagonal main crack extending from the loading point to the support, a secondary crack above the main crack, and a secondary crack below it.

This model is translated into equations as follows:

if $\rho_v > 0$ and $f \geq f_{ct}$:

$$w(V) = min(w_{tot}; w_{vy} + \frac{1}{3}(w_{tot} - w_{vy})) \tag{4.20}$$

otherwise :

$$w(V) = w_{tot} \tag{4.21}$$

with $w_{tot} = w(V)$ expressed in equation 4.13, w_{vy} and f expressed in equations 4.16 and 4.18 respectively.

Equations 4.20 and 4.21 can therefore be used to predict the width of the critical diagonal shear crack in a deep beam at each loading stage.

4.1.3.4 Measured vs predicted response of specimen I-03-2

To verify this new formulation of the prediction of the critical diagonal shear crack width as a function of the applied shear in a deep beam, a comparison is made between experimental (section 4.1.1) and predicted results.

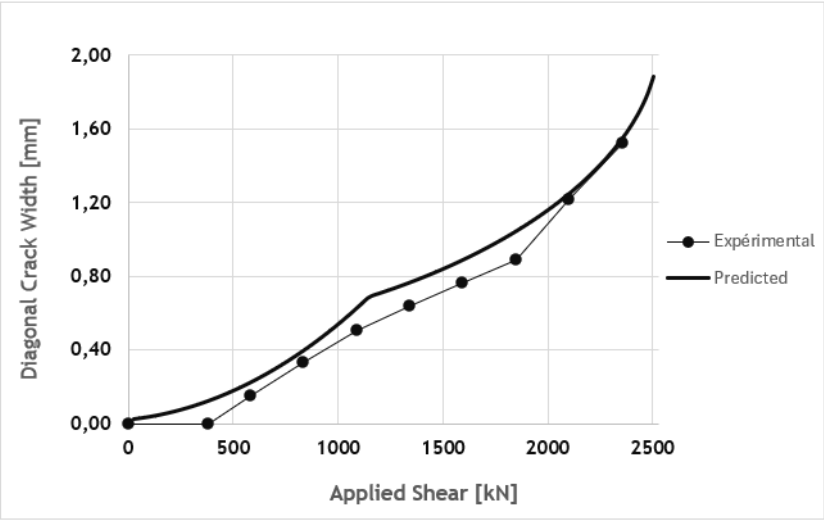

Figure 4.8: Measured and predicted crack widths for specimen I-03-2 including crack control effect.

Figure 4.8 shows a better accuracy of the predicted results, while remaining fairly conservative. Indeed, a close look at the experimental measurements reveals a drop in slope from an applied shear $V \approx 1200kN$. This decrease in slope reflects the effect of crack control, induced by the formation of secondary cracks. The table 4.3 below shows the improved accuracy of this second formulation of the predicted crack width w_{Pred2} following the applied shear V compared with that from the first formulation w_{Pred1}. Up to $V = 1088kN$, both formulations predict the same crack width values, which means that up to this load there are no secondary cracks, only the main crack widens. Beyond this load, secondary cracks form, and the rate of widening of the main crack decreases.

This crack control effect is well captured by the new model, as shown by the continue curve of predicted widths. There is therefore a better match between crack widths obtained experimentally and those predicted, and the second formulation can be retained.

$V/V_u[\%]$	$V[kN]$	$w_{Exp}[mm]$	w_{Pred1}	$w_{Pred2}[mm]$
0	0	0.00	0.00	0.00
15	380	0.00	0.13	0.13
23	582	0.15	0.22	0.22
33	835	0.33	0.39	0.39
43	1088	0.51	0.60	0.60
53	1341	0.64	0.87	0.75
63	1595	0.76	1.21	0.87
73	1848	0.89	1.64	1.01
83	2101	1.22	2.20	1.19
93	2354	1.52	3.01	1.47
100	2531	-	3.94	1.77

Table 4.3: Measured and predicted crack widths at each loading stage for specimen I-03-2 with and without crack control effect.

In order to further validate this model, the influence of main beam properties such as the amount of web reinforcement, the concrete strength and the shear span length will be

studied on sets of almost identical specimens varying only by the considered property, in order to determine its influence on the crack behavior. Then, predictions similar to the one shown in figure 4.8 will be made for other deep beams.

4.2 Test data

To further verify the crack-width prediction model formulated above, a total of 18 published tests on simply supported beams with a/d between 1.2 and 2.3 were used. These specimens were taken from the database used to validate the 2PKT model. In fact, only tests for which crack width measurements at different loading stages are provided, as well as the width of the loading plate l_{b1}, are retained. l_{b1} is an essential parameter for the prediction formulated here. Approximating it by orders of magnitude would lead to a loss of accuracy.

The table 4.4 below summarizes the main properties of the specimens under consideration, all properties required for a calculation being listed in the appendix.

Beam	$a/d[-]$	$d[mm]$	$\rho_l[\%]$	$\rho_v[\%]$	$f_c[Mpa]$	$V_{u,Exp}[kN]$
S0M	1.55	1095	0.70	0.0	34.2	721
S1M	1.55	1095	0.70	0.1	33	941
L0M	2.28	1095	0.70	0.0	29.1	416
L1M	2.28	1095	0.70	0.1	37.8	663
I-03-2	1.84	978	2.29	0.29	36.1	2531
I-02-2	1.84	978	2.29	0.2	27.2	2019
II-02-CCC1021	1.84	980	2.31	0.2	31.9	1463
II-03-CCT1021	1.84	980	2.31	0.31	30.4	2829
II-02-CCT0507	1.84	980	2.31	0.2	21.5	1784
III-1.85-02	1.84	980	2.31	0.2	28.3	2171
III-1.85-025	1.84	980	2.31	0.24	28.3	2295
III-1.85-03	1.84	980	2.31	0.29	34.4	1833
III-1.85-03b	1.84	980	2.31	0.31	22.8	2095
III-1.85-00	1.84	980	2.31	0.00	21.9	1624
III-1.2-03	1.20	980	2.31	0.31	29.1	3688
IV-2175-1.85-03	1.85	1750	2.37	0.31	34.0	3745
IV-2123-1.85-03	1.85	495	2.32	0.3	28.7	1463
IV-2123-1.85-02	1.85	495	2.32	0.2	29.1	1544

Table 4.4: Summary of main beam properties [1].

4.3 Validation

4.3.1 Influence of web reinforcement

As presented above, crack control in a beam is mainly induced by the amount of web reinforcement. In fact, web reinforcement force the formation of secondary cracks all around the main diagonal crack. As a result, the main diagonal crack widens less at each loading stage following the appearance of secondary cracks.

To validate this, a comparative study of crack patterns following loading of specimens III-1.85-00 and III-1.85-03b listed in the table 4.4 is carried out. These two specimens are almost identical, and vary only in the amount of web reinforcement. specimen III-1.85-00 has no web reinforcement while III-1.85-03b has $\rho_v = 0.31\%$ of transverse reinforcement and $\rho_h = 0.29\%$ of horizontal reinforcement.

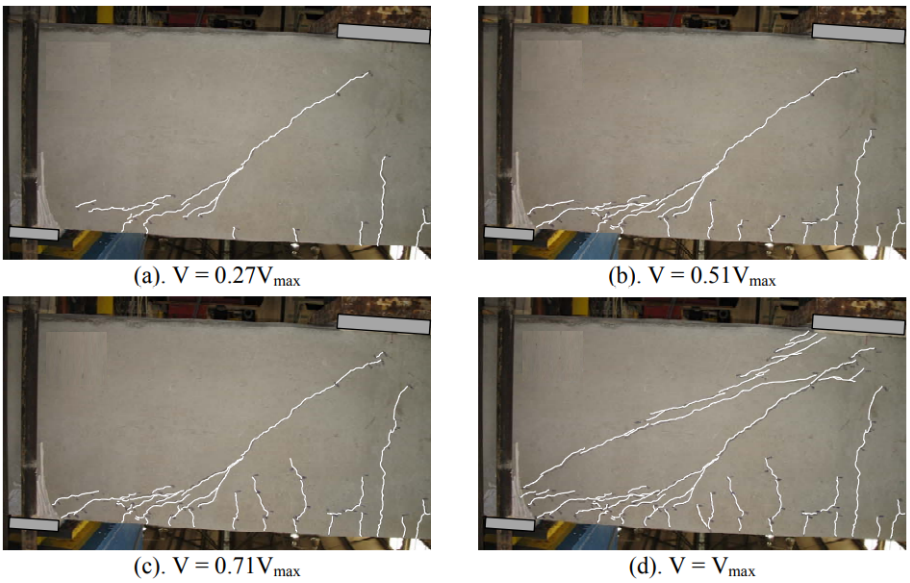

Figure 4.9: Crack development in specimen without web reinforcement, III-1.85-00 [3].

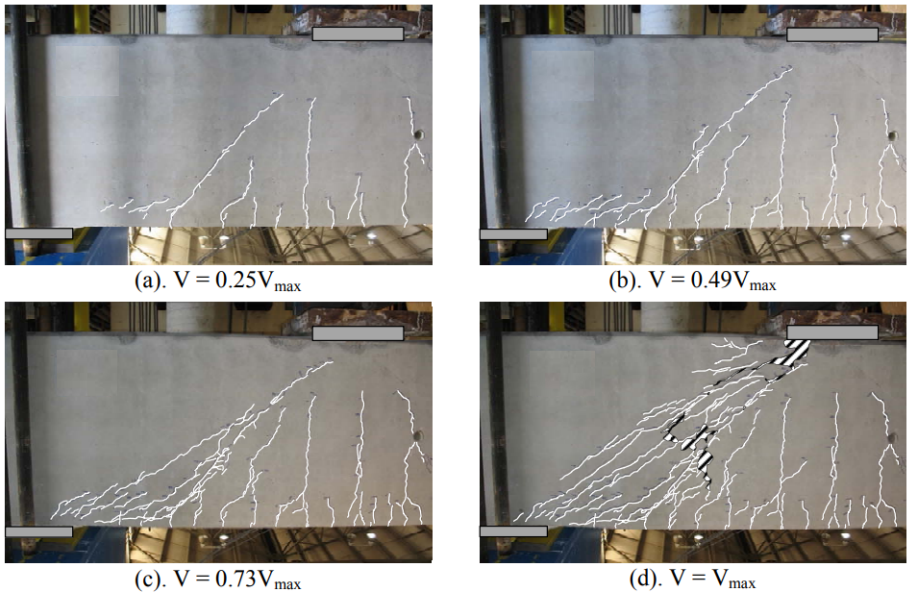

Figure 4.10: Crack development in specimen with 0.3% in each direction, III-1.85-03b [3].

Figures 4.9 and 4.10 show the evolution of cracks in these two beams during experimental tests. It is clearly visible that test III-1.85-03b shows significantly more cracks than test III-1.85-00 at the same loading levels. At the maximum applied shear, test III-1.85-03b shows a fairly rich cracking pattern with a main diagonal crack that is difficult to distinguish as it is well surrounded by secondary cracks, in contrast to test III-1.85-00 where at the same percent of maximum applied shear the main diagonal crack is quite distinct given the reduced number of secondary cracks.

Measurements of the width of the main diagonal crack at different loading levels were taken at each of the two tests. They are compared in the figure 4.11 below.

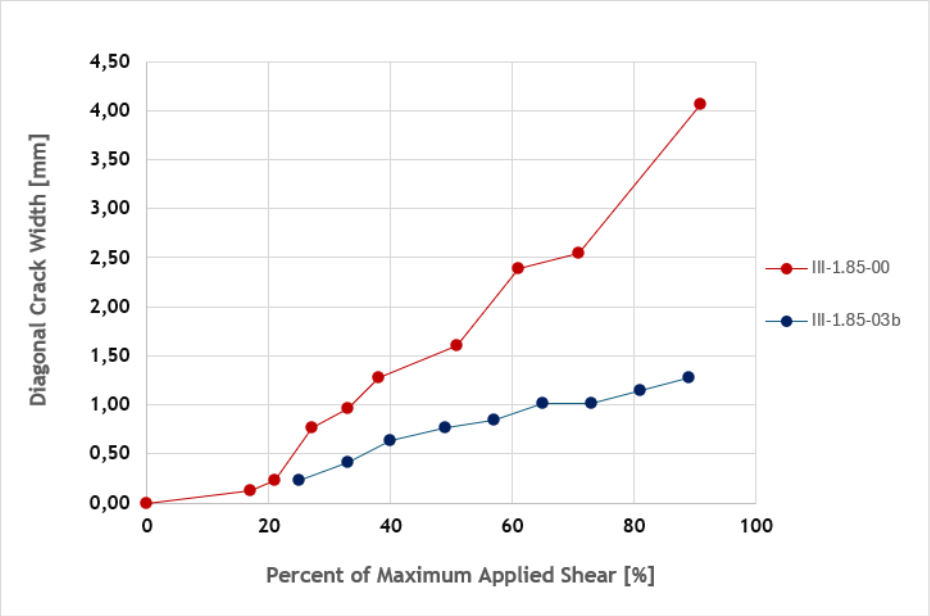

Figure 4.11: Diagonal crack widths comparison of III-1.85-00 and III-1.85-03b.

As shown in figure 4.11, the main diagonal crack widens less for the specimen with approximately 0.3% of web reinforcement. This reflects the crack control effect induced mainly

by web reinforcement (transverse and horizontal reinforcement) as explained above.

These experimental measurements can then be compared with the crack widths predicted by the model on the same specimens.

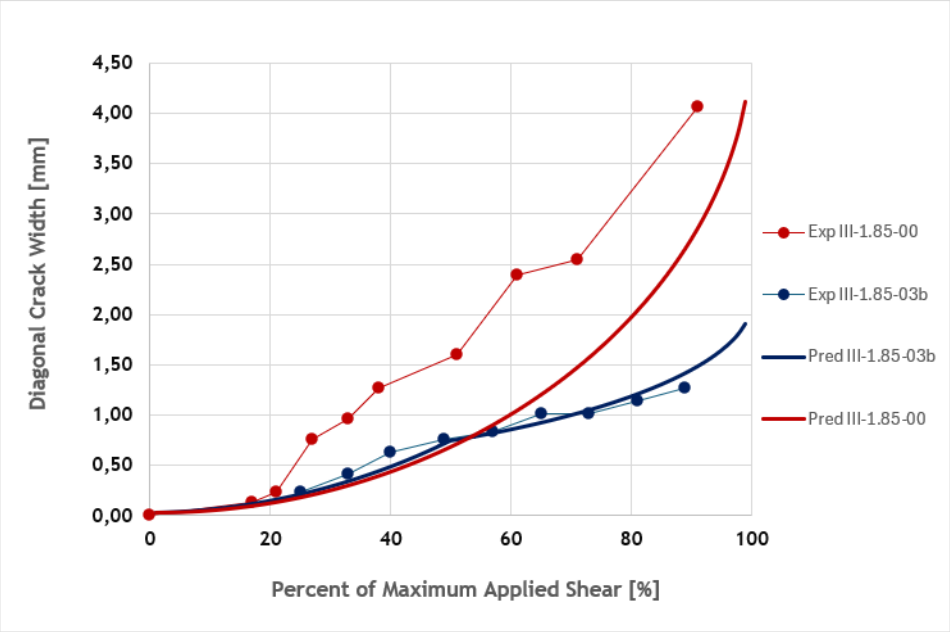

Figure 4.12: Measured and predicted diagonal crack widths of III-1.85-00 and III-1.85-03b.

Figure 4.12 therefore shows that the effect of crack control is well taken into account in the prediction of widths of the main diagonal crack in specimen III-1.85-03b, as the experimental measurements match the calculations fairly well. The prediction curves of the two specimens are approximately merged until the clear formation of secondary cracks in III-1.85-03b, which results in the "break" in its curve, at approximately $V/V_u = 0.5$. This observation is validated by comparing figures 4.9 and 4.10 where a clear difference in the crack patterns of the two specimens is observed at $V = 0.5V_{max}$ (figures 4.9b and 4.10b). This shows that the appearance of secondary cracks, and hence crack control, is mainly due to the web reinforcement.

To further validate this analysis, figure 4.13 below is prepared. It compares the experimental and predicted evolution of the width of the main diagonal crack following the applied shear on specimens III-1.85-02, III-1.85-025, III-1.85-03 and III-1.85-03b listed in the table 4.4. These beams vary mainly by the amount of web reinforcement. Specimen III-1.85-03b is the main exception with a concrete strength f_c quite lower than those of the other three specimens.

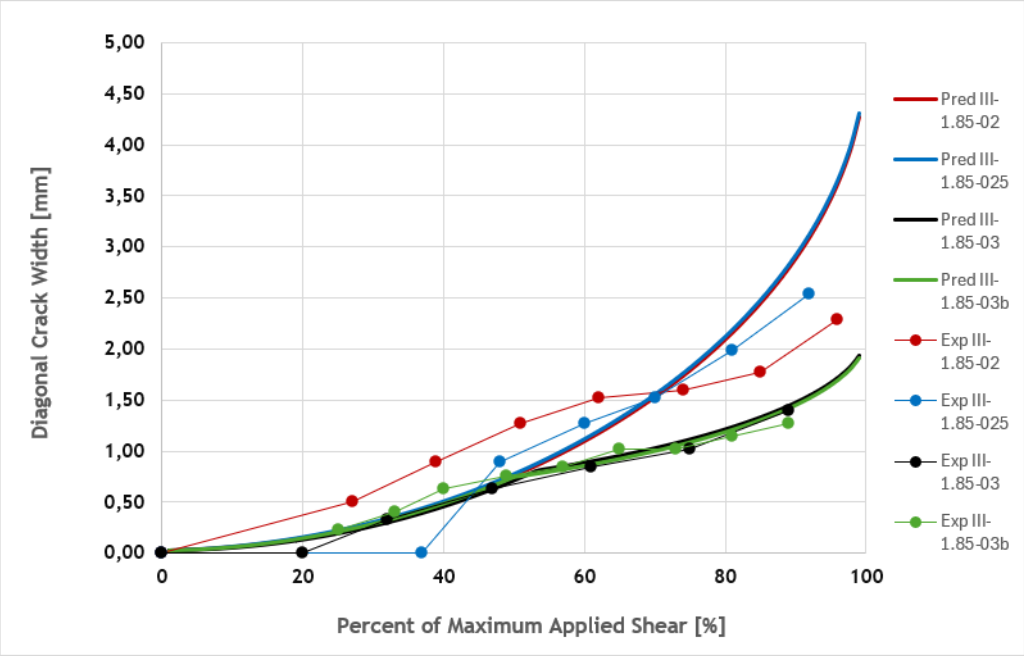

Figure 4.13: Measured and predicted diagonal crack widths of four almost identical specimens with the web reinforcement ratio as the main variable.

This figure shows fairly good agreement between experimental measurements and predictions of the width of the main diagonal crack at each loading stage, further evidence of the accuracy of the model developed. The crack control effect is well captured. Indeed, predicted curves of the four specimens are almost all superposed until the formation of secondary cracks (at the location of the "break") in specimens III-1.85-03 and III-1.85-03b, despite the variability in the amount of web reinforcement. Thus, the amount of web reinforcement only influences the evolution of crack width after the formation of secondary cracks, if of course the total tensile stress induced within the main crack mainly by the yielding of the web reinforcement is sufficient to form secondary cracks. This is shown by the superposition of the four prediction curves up to the "break" and the total superposition of those of specimens III-1.85-02 and III-1.85-025, despite a 0.05% difference between their web reinforcement ratios.

4.3.2 Influence of concrete strength

Figure 4.13 also shows the limited influence of concrete compressive strength on main crack widening. Indeed, specimen III-1.85-03b benefits from a crack control effect unlike specimens III-1.85-02 and III-1.85-025 despite the fact that its concrete strength is 5.5$[Mpa]$ lower than that of the other two. It is deduced that the crack-control effect is mainly due to a sufficient quantity of web reinforcement before the concrete strength. Also, the predicted curves of specimens III-1.85-03 and III-1.85-03b are almost identical despite a difference of approximately 12$[Mpa]$ between their concrete strengths. Concrete strength therefore has a limited influence compared to that of the amount of web reinforcement on the evolution of the width of the main diagonal crack in a deep beam following its loading.

4.3.3 Influence of shear span length

The shear span a is an important property of beams, both in experimental studies and in predictions. In the latter, it is used to calculate the minimum strain along bottom longitudinal reinforcement $\epsilon_{t,min}$ at each loading stage, as shown by equation 4.13. This predicts the increase in the width w of the main diagonal crack with the increase in the shear span. However, this increase should be relatively small for a shear span as the main variable, since it only influences the contribution of the bottom longitudinal reinforcement to the crack width (the second term of equation 4.13), which is small compared to that of the vertical shear displacement Δ_c (the first term of the equation 4.13) in deep beams.

The influence of the shear span length is captured by analysis of tests III-1.85-03 and III-1.2-03 listed in table 4.4. These two specimens are almost identical in every respect, and vary mainly in the a/d ratio and therefore in the shear span which is $a = 1804[mm]$ for III-1.85-03 and $a = 1177[mm]$ for III-1.2-03; since the effective depth of section $d = 980[mm]$ in both cases.

Figure 4.14: Crack patterns at shear failure in specimens III-1.85-03 (left) and III-1.2-03 (right) [3].

Figure 4.14 above compares crack patterns at shear failure in tests III-1.85-03 and III-1.2-03. Despite the clear difference in shear spans, it is difficult to distinguish the cracking patterns at failure.

A comparison of main diagonal crack width measurements at different loading stages for each of these specimens is shown in figure 4.15 below.

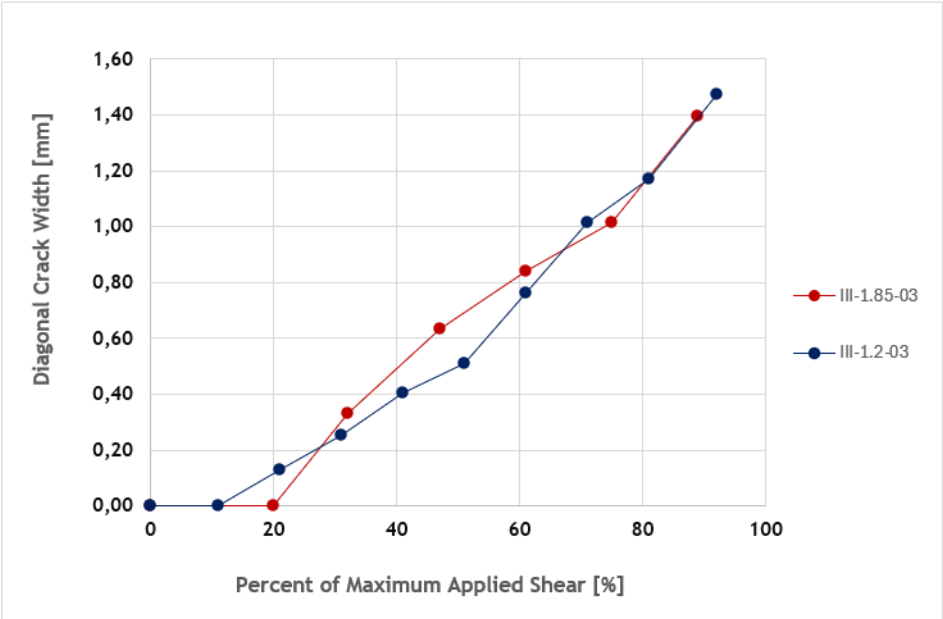

Figure 4.15: Diagonal crack widths comparison of III-1.85-03 and III-1.2-03.

As shown in the figure above, specimen III-1.85-03 exhibits a thicker crack than specimen III-1.2-03 at almost all loading levels due to its greater shear span. However this difference is relatively small.

The origin of this difference is fairly well captured by the prediction model, as shown in figure 4.16.

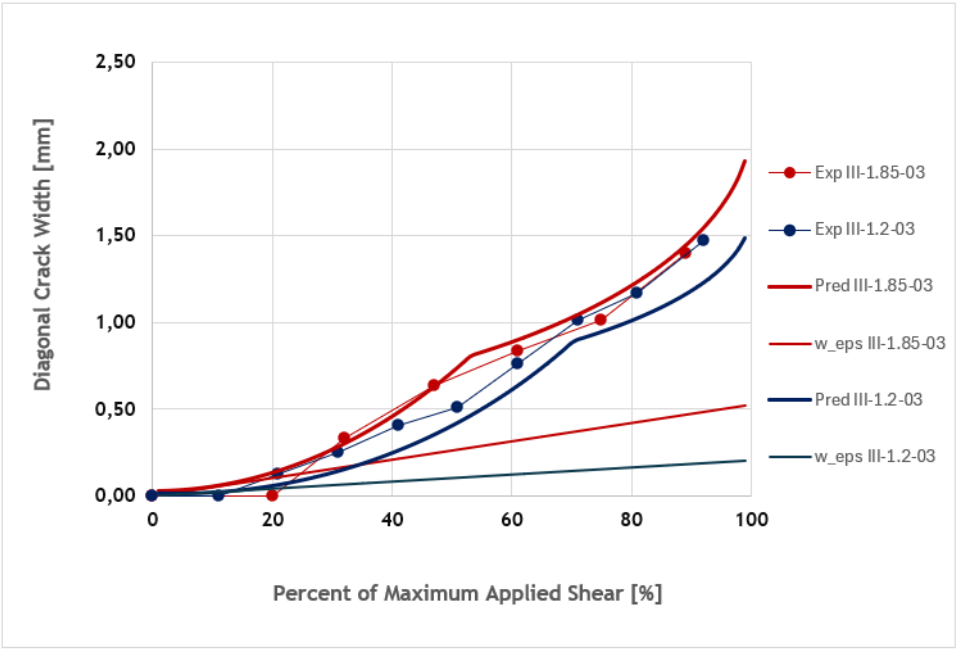

Figure 4.16: Measured and predicted diagonal crack widths of III-1.85-03 and III-1.2-03.

The "w_{-eps}" curves in the figure above represent the second term of the equation 4.13, i.e. the contribution to crack width from the bottom longitudinal reinforcement. The gap between these curves corresponds approximately to the gap between the prediction curves,

slightly overestimated. Thus, the shear span only affects the contribution of the bottom longitudinal reinforcement to crack width, but only slightly, as this contribution is the smaller of the two contributions to the crack width.

Figure 4.16 also shows a good matching between experimental measurements and predictions. Thus, the prediction model developed is quite accurate and captures well the influence of the shear span length on the widening of the main diagonal crack of a deep beam following its loading.

4.3.4 Validation with Tests

Finally, the model for the prediction of the width w of the critical diagonal shear crack following the applied shear V presented in section 4.1.3 is then implemented on the different specimens listed in table 4.4. A curve similar to that shown in figure 4.8 is predicted for each of these deep beams in order to compare the results predicted by the equations 4.20-4.21 and those obtained experimentally, and thus to further validate the model developed.

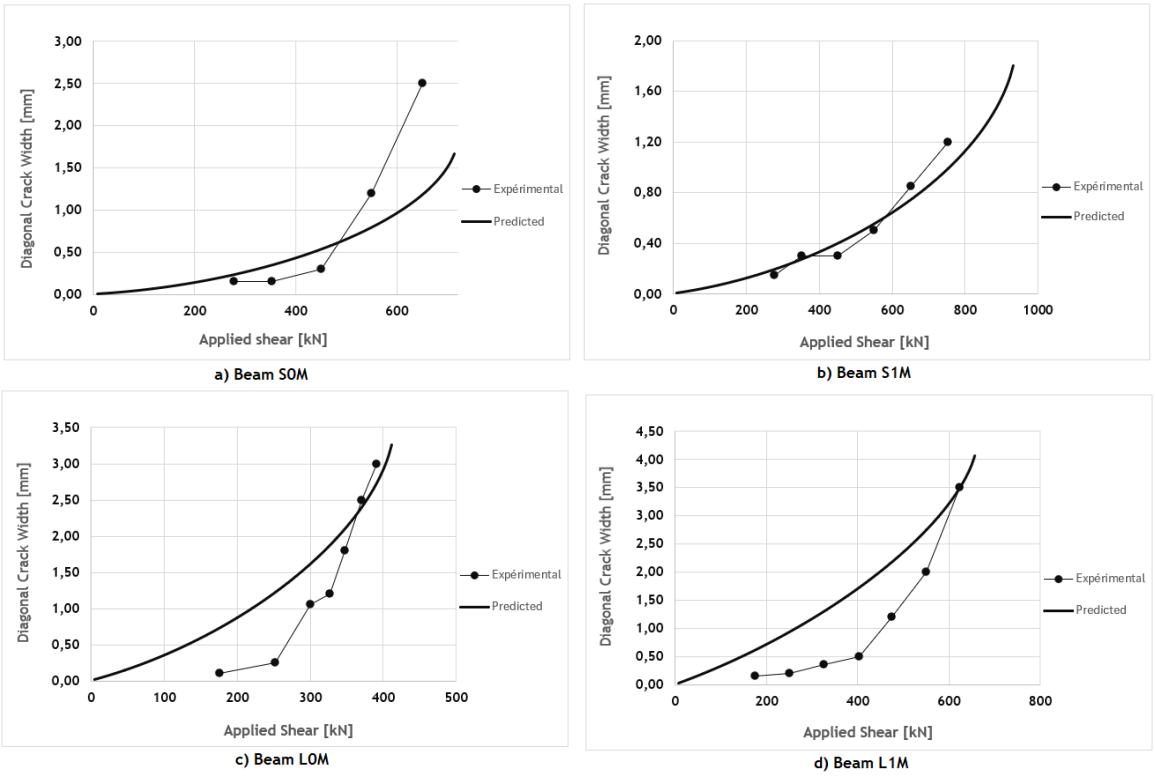

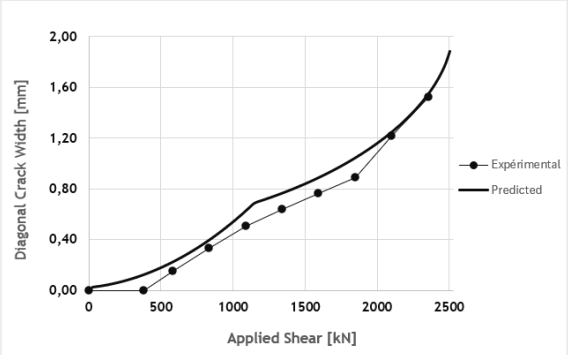

e) Beam I-03-2

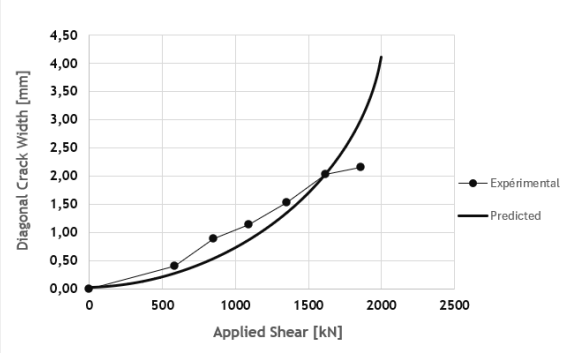

f) Beam I-02-2

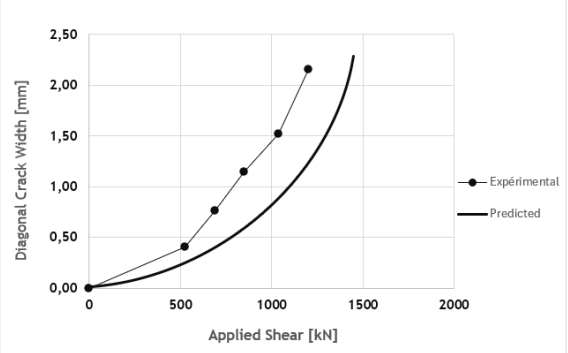

g) Beam II-02-CCC1021

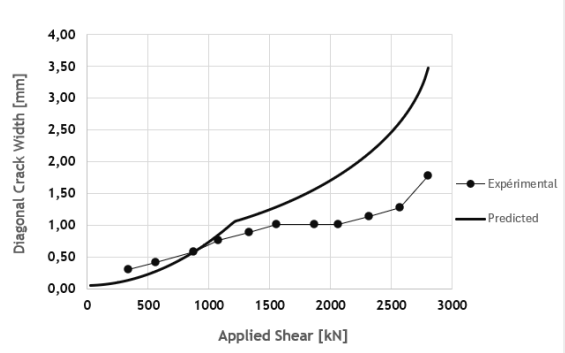

h) Beam II-03-CCT1021

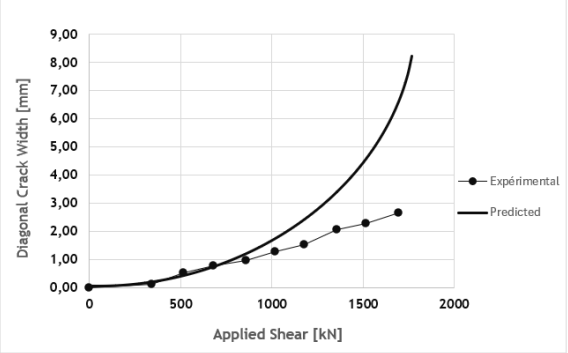

i) Beam II-02-CCT0507

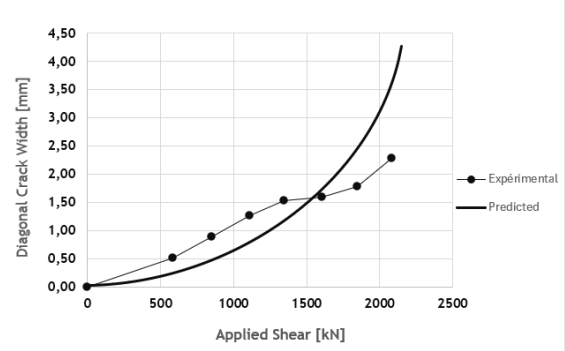

j) Beam III-1.85-02

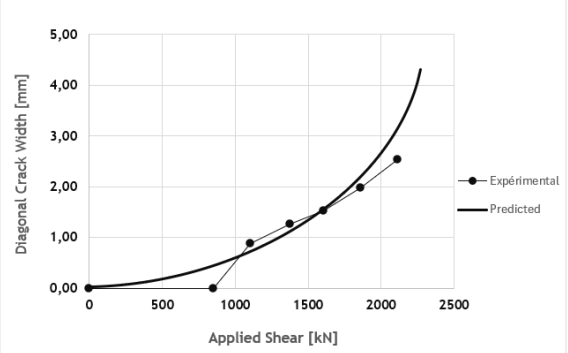

k) Beam III-1.85-025

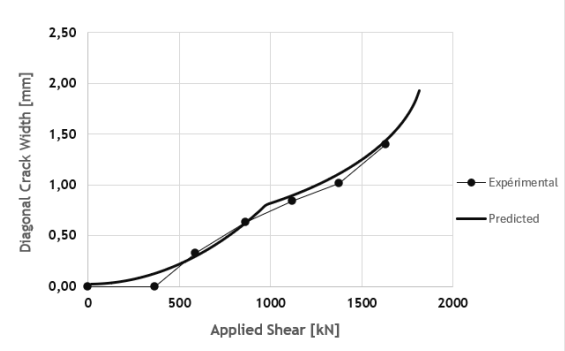

l) Beam III-1.85-03

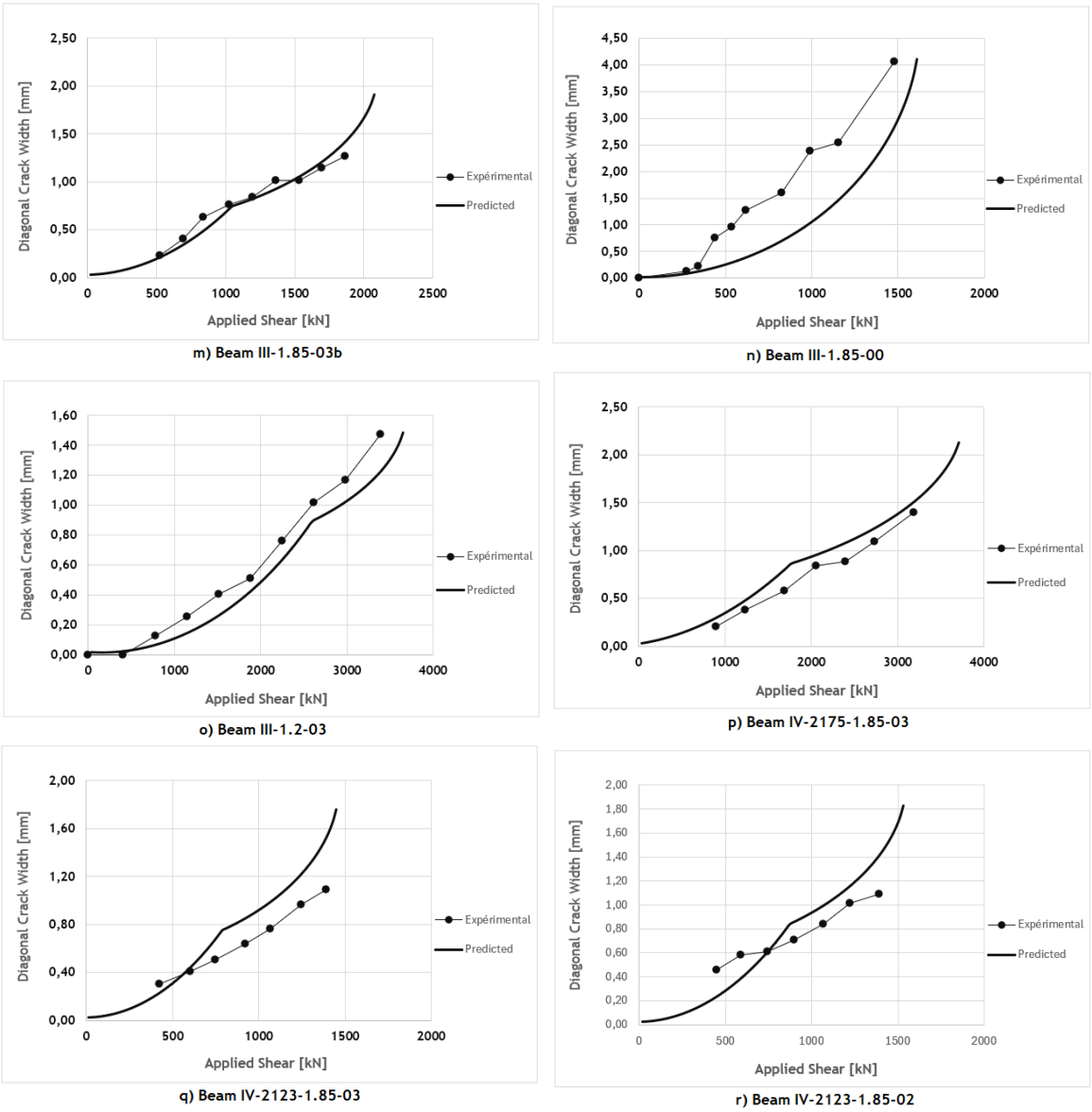

Figure 4.17: Measured and predicted maximum crack widths for 18 tests.

Figure 4.17 shows validations of the proposed approach on the prediction of the maximum crack width as a function of the applied shear with the tests from table 4.4. Predicted results are fairly accurate compared with those obtained experimentally. Equations 4.20 and 4.21 capture well the crack control effect when it is present.

Firstly, figure 4.17a, 4.17c and 4.17n respectively for specimens S0M, L0M and III-1.85-00 show experimentally a fairly rapid widening of the main diagonal crack. Predictions match this as closely as possible. These beams do not have stirrups, and the approach developed therefore considers that there is no formation of secondary cracks and therefore no crack control effect. Only the main diagonal crack widens, and its width predicted by equation 4.21 is greater than that predicted by equation 4.20 which considers a crack control.

Beams S1M, L1M, I-02-2, II-02-CCC1021, II-02-CCT0207, III-1.85-02 and III-1.85-025 on the other hand, have transverse reinforcement. However, they do not exhibit crack control. Indeed, for these specimens, the total tensile stress generated in the vicinity of the critical diagonal crack after yielding of stirrups, i.e. when $w = w_{vy}$, is not sufficient enough

to form secondary cracks ($f \leq f_{ct}$). Thus, the prediction model developed considers only the presence of the main crack, whose width is calculated through equation 4.21. Figures for these specimens show that the experimental results are more or less in line with those predicted, particularly for specimens S1M in figure 4.17b and III-1.85-025 in figure 4.17k. Here again, the model for the prediction of the width of the critical diagonal shear crack gives fairly accurate results, given the complexity of the problem.

Finally, all other specimens that feature also transverse reinforcement benefit from a crack-control effect, which can be seen through the "break" in their predicted crack-width curve. For these beams, the total tensile stress f is greater than the tensile strength of the concrete f_{ct}. Thus, when the width of the main crack w reaches the width of the crack following the yielding of the stirrups w_{vy}, the model predicts the formation of secondary cracks, and hence a reduction in the rate of widening of the main crack, expressed by a decrease in the slope of the predicted curve after the "break". Figures relating to these specimens also show a fairly good match between experimental results and predictions, as do figures 4.17e, 4.17l, and 4.17m related to specimens I-03-2, III-1.85-03 and III-1.85-03b. The approach of predicting the maximum crack width as a function of the applied shear on the beam therefore gives fairly accurate results in these cases too.

The model formulated in this work can therefore be validated on the basis of these 18 tests.

4.4 Discussion

The proposed approach on the prediction of the critical shear crack width at each loading stage is based on the CBA-2PKT model. To improve the accuracy of the results, it takes into account the crack control effect induced by the formation of secondary cracks on either side of the main crack, which is generally the case for deep beams with sufficient web reinforcement. This model is validated on the basis of 18 published tests on simply supported beams for which measurements of maximum crack width have been carried out at different loading stages. Thus, this approach enables the estimation in advance of the maximum crack width that will occur on the beam, depending on its main properties and knowing the load it is expected to support. Since the model is conservative in the majority of cases, if the predicted maximum crack width is less than the set limit, the beam can continue to be used as it is. On the other hand, if the predicted maximum crack width is greater than the set limit, action should be taken: either a more precise analysis should be carried out to estimate the maximum width even more accurately, or maintenance measures should be taken to ensure the beam's compliance with the serviceability limit states.

However, this study does not take into account long-term effects such as fatigue and creep, as well as the influence of the environment. Indeed, unlike the CBA model presented above, where predictions are made on the basis of on-site measurements where long-term effects are represented in these measurements and therefore indirectly influence the predictions, the model developed here does not consider any on-site measurements, which is precisely its basic purpose, i.e. to make predictions "in advance". So, in order to achieve a more accurate analysis and to predict crack widths closer to those that would be observed in reality, long-term effects should be incorporated into the model. This could be achieved, for example, by carrying out measurements on the beam in its current state, such as the state of deformation of the critical loading zone and the vertical displacement of the diagonal crack

$w_{v,cr}$, and on the basis of these predict a maximum crack width according to the future load the beam will have to support. The inclusion of long-term effects in a predictive crack-width model is an improvement perspective for the model developed in this work.

The approach proposed in this work is nevertheless quite satisfactory, given the complexity of the problem. Accurate calculation of the crack width on a beam is quite difficult. Long-term effects such as fatigue and creep are difficult to model and to integrate into a study, and other external parameters such as environmental ones influence the condition of the beam in service. However, given these complexities and uncertainties, the predictive model developed here gives fairly accurate results, including such a complex mechanism as crack control effect.

Chapter 5

Conclusions and perspectives

The work deals with deep beams at ultimate limit states and at the service limit states.

The ultimate limit state (ULS) study can be summarized as follows:

- The approach developed is a simplified model of the Two-Parameter Kinematic Theory (2PKT) for Shear Behavior of Deep Beams which makes it possible to describe the deformed shape of such members in terms of just two primary parameters given that in the case of deep beams the fundamental hypothesis that "plane sections remain plane" is no longer respected. And so, to predict the shear strength and deformations patterns of deep beams at shear failure, as in the case of slender beams.

- The simplifications made to the initial model mainly consist in developing a non-iterative model whose shear design equations are closed and fairly simple to implement. The complete 2PKT model is iterative, mainly through the determination of the minimum strain along bottom longitudinal reinforcement (one of the two degrees of freedom) which depends on the beam's shear strength, and the equations predicting the shear strength components depend on parameters whose expressions are rather cumbersome, necessitating prior calculations. In the simplified approach, the determination of the minimum strain along bottom longitudinal reinforcement is direct, and the expressions of the various parameters on which the shear strength components depend are simplified, with a view to dispensing with previous calculations and having simple closed-form shear design equations as in the case of slender beams.

- Simplifying the initial model, however, leads to a loss of precision. It is therefore necessary to find a good compromise between simplicity and accuracy. In the end, the accuracy of this new approach is good, given the simplicity provided. It is validated on the basis of 327 published tests on simply supported beams with a/d between 0.5 and 2.5 whose coefficient of variation of the ratios of experimental to predicted shear strengths following the simplified approach is 18.81% with an average of 1.26, compared with a coefficient of variation of the ratios of 13.72% with an average of 1.11 between the experimental strengths and that predicted by the full 2PKT model. In comparison, this simplified approach is still more accurate than AASHTO and ACI codes whose coefficients of variation of the ratios between experimental and predicted results are 24.6% and 29.0% respectively.

The serviceability limit state (SLS) study can be summarized as follows:

- The proposed model is inspired by a rapid crack-based assessment approach, which enables to assess the residual shear capacity of a deep beam on the basis of only three input parameters and two simple closed-form equations, and by the 2PKT model studied at ULS. However, at SLS, interest is generally directed towards assessing crack widths, so that appropriate measures can be taken to prevent unacceptable degradation of the beam and ensure its suitability for service. Thus, the designed model enables to predict the maximum crack width that would appear on a deep beam in service at each loading phase, which is quite a complex task given the great variability of the effects influencing the evolution of cracks on a beam in service.

- The model is then designed in two phases. The first formulation considers only one crack, the critical diagonal shear crack, whose maximum width is expressed in the 2PKT model. However, this formulation does not take into account the formation of secondary cracks on either side of the main crack, which can lead to crack control in certain cases. Indeed, with the formation of secondary cracks, the widening of the main crack is reduced. The second formulation builds on the first by incorporating this crack control effect. It considers that when the total tensile stress induced in the vicinity of the main crack following the yielding of the transverse reinforcement is greater than the tensile strength of the concrete, secondary cracks form and the rate of widening of the main crack is reduced, which is reflected in the curves expressing the maximum width of the main crack as a function of the applied shear by a decrease in the slope of the curve after the width of the main crack has reached that following yielding of the transverse reinforcement.

- This second formulation of the prediction of the maximum width of the critical diagonal shear crack is validated on the basis of 18 published tests on simply supported beams for which measurements of maximum crack widths were made at different loading stages.

The work carried out nevertheless opens up on other effects to consider. At ULS, the simplicity of the shear design equations is quite satisfactory, but the accuracy could be improved by taking a better account of the size effect, which a good understanding is a key purpose of the 2PKT model. Further study could therefore be carried out on beams at the boundary between deep and slender.

At SLS, on the other hand, long-term effects such as fatigue, creep and environmental impact influencing the evolution of cracks on a beam in service have not been taken into account in the present model. In some cases, they can accelerate crack growth and beam degradation. Taking into account these effects, which are admittedly rather complex to model, would make the predictions more conservative and accurate.

Bibliography

[1] Boyan I. Mihaylov, Evan C. Bentz, and Michael P. Collins "Two-Parameter Kinematic Theory for Shear Behavior of Deep Beams".
In : *ACI Stuctural Journal* (June 2013).
DOI: http://doi.org/10.14359/51685602.

[2] Boyan Mihaylov, Eissa Fathalla, Alexandru Trandafir "Rapid crack-based assessment of deep beams based on a single crack measurement".
In : *Engineering Structures 322* (September 2024).
DOI: https://doi.org/10.1016/j.engstruct.2024.119054.

[3] David Birrcher, Robin Tuchscherer, Matt Huizinga, Oguzhan Bayrak, Sharon Wood, and James Jirsa "Strength and Serviceability Design of Reinforced Concrete Deep Beams".
In : *CTR Technical Report 0-5253-1* (April 2009).

[4] Jarrod Zaborac, Apostolos Athanasiou, Salvatore Salamone, Oguzhan Bayrak, and Trevor Hrynyk "Evaluation of Structural Cracking in Concrete".
In : *CTR Technical Report 0-6919-1* (April 2019).

[5] Boyan Mihaylov "Model for rapid evaluation of corner crack widths in reinforced concrete dapped-end conections".
In : *Engineering Structures 303* (January 2024).
DOI: https://doi.org/10.1016/j.engstruct.2024.117497